Validation and verification of the new aerodynamics in Bladed 4.8 and later

Document No. 110052-UKBR-19, Rev. C
Date of issue: November 2021

Garrad Hassan & Partners Ltd

Project name:	Validation and verification of the new aerodynamics in Bladed	DNV GL Energy
		One Linear Park
Report title:	Technical report	Temple Quay
Customer:		Bristol
Contact person:		BS2 0PS
Date of issue:	November 2021	
Report No.:	110052-UKBR-19, Rev. C	

Prepared by:

Menno Kloosterman
Engineer Turbine Engineering

[Name]
[title]

[Name]
[title]

Verified by:

Patrick Rainey
Bladed Product Manager

David Langston
Engineer Turbine Engineering

William Collier
Senior Engineer, Bladed Development

Approved by:

Patrick Rainey
Bladed Product Manager

☐ Strictly Confidential
☐ Private and Confidential
☐ Commercial in Confidence
☐ DNV GL only
☒ Client's Discretion
☐ Published

Keywords:
wind energy, wind turbine, power curve, aerodynamic blade design

Reference to part of this report which may lead to misinterpretation is not permissible.

Rev. No.	Date	Reason for Issue	Prepared by	Verified by	Approved by
A	13-02-2017	First issue	Menno Kloosterman	Patrick Rainey, David Langston	
B	August 2018	Modified impulsive lift verification, added verification of old-aero style dynamic stall model.	Menno Kloosterman	Stephen Parkinson	
C	November 2021	Added structural velocity in induction calculations	Galih Bangga	Steven Parkinson	

Verification and validation of the new aerodynamics in Bladed 4.8

1   NOMENCLATURE

α	Angle of attack
c	Chord length
C_d	Drag coefficient
C_l	Lift coefficient
C_m	Pitching moment coefficient
C_n	Normal force coefficient
M	Mach number
V_∞	Ambient wind speed

Beddoes-Leishman constants

T_f	Separation time constant
T_p	Pressure lift time constant
T_v	Vortex lift time constant
T_{vl}	Vortex travel time constant
$A_{i=1,2,3,4}$	Indicial response function coefficients
$b_{i=1,2,3,4,5}$	Indicial response function exponents

2   INTRODUCTION

This report presents the results of validation and verification work carried out for the "new aerodynamics" module that was released in Bladed 4.7 as a beta, and as a default module in Bladed 4.8. The theoretical background of the model can be found in reference /11/.

From Bladed version 4.8 onwards the new aerodynamics module completely replaces the default implementation that is used in older versions of Bladed (3.x and 4.0-4.7) herein referred to as "old aerodynamics".

The main focus of this report is to:

1. Provide evidence of model verification on the new aerodynamics implementation that is now the default modelling option in the latest versions of Bladed (from version 4.8 onwards).

2. Highlight the different modelling assumptions made in the new aerodynamics implementation.

3. Illustrate and provide explanation for differences between the old and new aerodynamic formulations via comparison of both steady state and dynamic simulations.

The remainder of the report is structured as follows. Section 3 discusses the result of a comparison between the old and new aerodynamics module for steady state calculations. The sub models for dynamic stall and dynamic wake are verified against analytical solutions and measurements in isolation in Section 4. In section 5, results of a code comparison exercise are provided from DNV GLs involvement in the MexNext consortium (reference /6/). In the code comparison, the predictions of the new aerodynamics code and lifting line code are compared against the NASA-AMES measurements in yaw. Results of this exercise are presented in Section 0. Section 6 presents a comparison of the fatigue and extreme loads between old and new aerodynamics based on full sets of load cases. The turbine models used represent modern day multi-MW turbines that DNV GL has analysed in commercial projects. Finally, Section 7 provides a validation of the new aerodynamics in combination with the non-linear blade model against measurements from the GE 6MW Haliade turbine.

2.1   Summary of Significant Results Differences

In Section 6, a detailed study and discussion is performed on a full set of load calculations. A brief summary of major differences between old aerodynamics and the default settings for the new aerodynamics is given here:

1. **Aerofoil orientation**: In the old aerodynamics, aerofoils were oriented perpendicular to the coned rotor plane, whereas with the new aerodynamics they are perpendicular to the local *deflected* neutral axis. This results in a difference in resolved inflow velocities for blades that have significant pre-bend or deflection. An option is however available in new aerodynamics to assume, equivalent to old aerodynamics, that the aerofoils are perpendicular to the coned rotor plane. With this option enabled for large flexible blades, the new aerodynamics results align more closely with the old aerodynamics results.

2. **Skew wake**: Results in yawed flow are affected by the settings "Momentum theory" and "Skew wake correction model". The first option mainly influences mass the mass flow through the rotor during operationg in yawed flow. This can influence the power production predictions as exemplified in Section 6.8. The option "Skew wake correction model" influences the distribution of inflow parameters across the rotor. This can have an impact on the yawing moment predictions. The effect of the skew wake model on turbine fatigue and extreme loads is however not studied in isolation in this report.

3. **Deep stall conditions**: In idling storm conditions, with yaw misalignments of 20-30° yaw misalignment, the dynamic stall models in the new aerodynamics have lower aerodynamic damping. Although the *aerodynamic* damping in such cases is often negative in both versions of the aerodynamics, the structural damping of the modes is usually sufficient to keep the blade stable in old aerodynamics but not sufficient in the new aerodynamics. The damping is significantly influenced by implementation details of the Beddoes-Leishman model. A detailed analysis is presented in Section 6.4.

4. **Slower decay in dynamic wake**: The dynamic wake models in the new aerodynamics (particularly the Øye model) predict a slower decay in aerodynamic torque following a step change in pitch or wind speed compared to the old aerodynamics. This can have the effect of reducing closed loop stability of the pitch-speed control and if the controller is tuned to have fairly low stability margins this can lead to significant increases in loads. In particular this can sometimes cause large differences in deterministic gust cases. The different decay times between the models are discussed in Section 4.2.

5. **Linearisation**: Aerodynamic states relating to dynamic stall and wake can now be included in the state-space analysis for Campbell diagrams and model linearisations. The implications and recommended practises are separately discussed in reference /13/.

3 STEADY STATE CALCULATIONS

The steady calculations are conducted with the demo_a blade (as provided by the Bladed installer) and the DTU 10MW reference wind turbine, with 7 blade modes enabled.

3.1 Performance coefficients

Performance coefficients results for a rigid rotor using the demo_a turbine are shown in Figure 3-1. The old and new aerodynamic models produce nearly identical results in power coefficient and thrust coefficient. A maximum difference of 0.25% is found between the old and new aerodynamics when looking at the maximum power coefficient for various pitch angles.
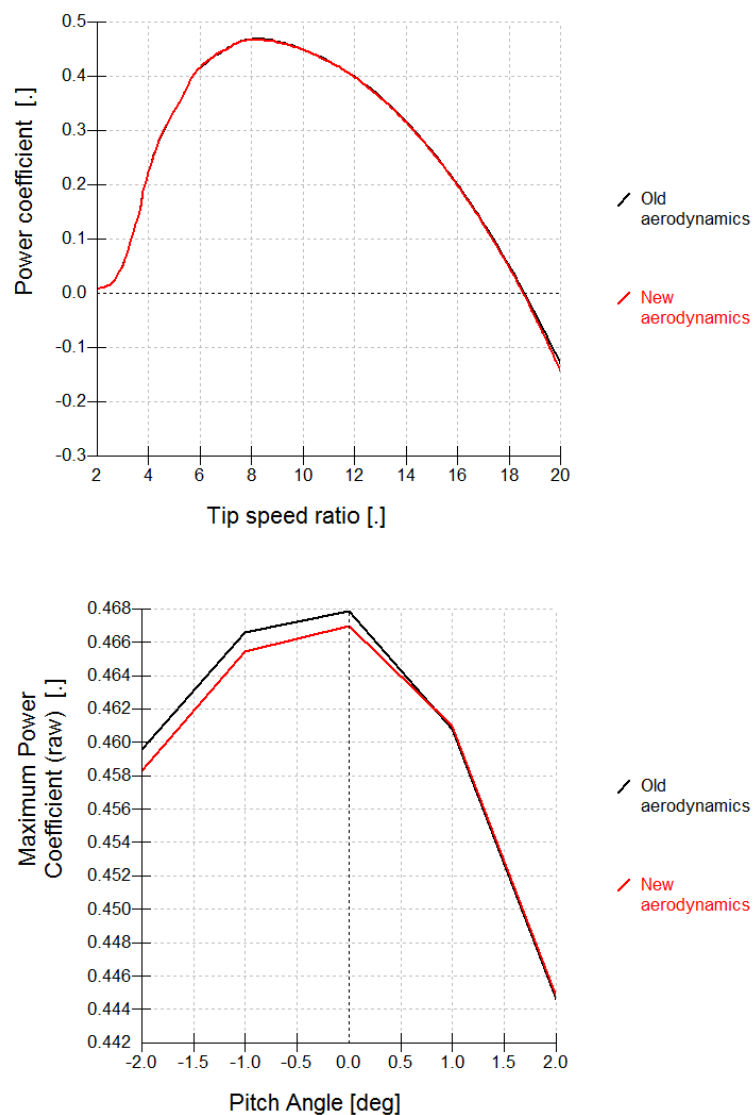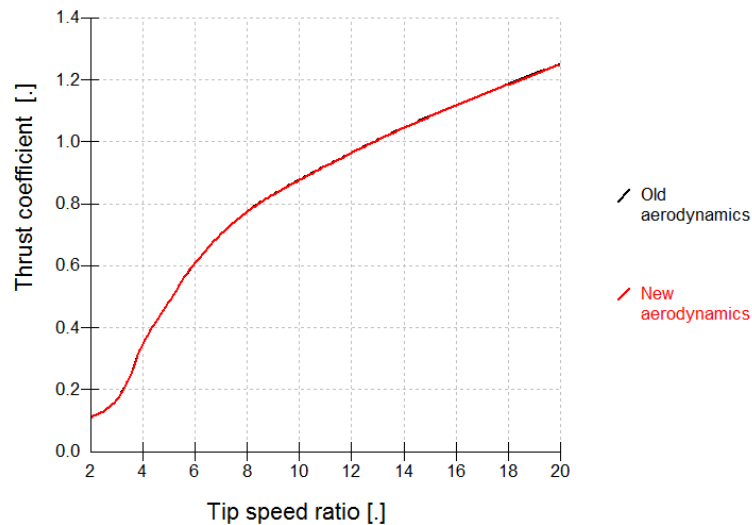
Figure 3-1 Comparison of performance coefficients between old and new aerodynamics for a rigid demo_a rotor

The DTU rotor has a more detailed blade definition including a torsional degree of freedom. With the new aerodynamics the blade flexibility can be included in the performance coefficients calculation. Figure 3-2 shows the comparison in power coefficient.
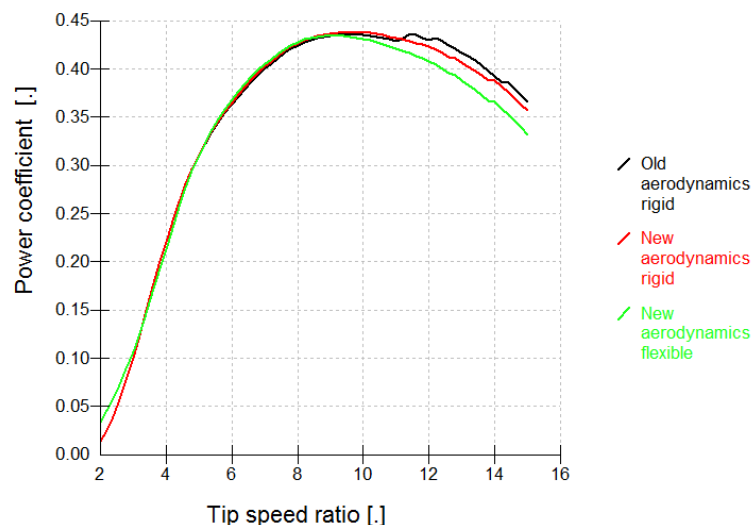

Figure 3-2 Comparison of performance coefficients between old and new aerodynamics for DTU 10MW blade rotor speed=9.6 rpm, pitch =0°

- For a rigid rotor the differences in maximum power coefficient are 0.3%. This reduces to 0.03% when the rotor is modelled with no tilt or cone.

- Modelling blade flexibilities slightly shifts the optimal tip speed ratio to the left and reduces the maximum power coefficient by 0.25%.

- Above a tip speed ratio of ~11 a more significant difference in power coefficient occurs. Figure 3-3 shows that at 20m along the blade a sudden change in angle of attack occurs. This appears to be caused by an aerofoil section with abrupt stalling characteristics leading to a difference in convergence between the old and new aerodynamics.
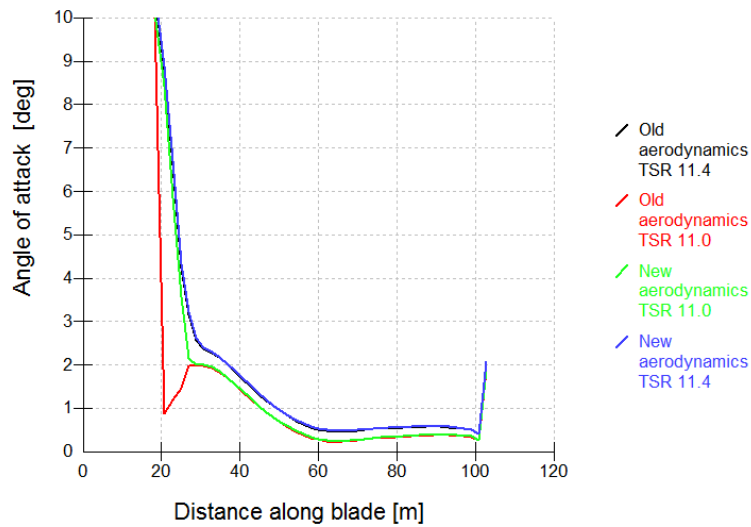
Figure 3-3 comparison in angle of attack between TSR=11 and TSR=11.4, rotor speed = 9.6, pitch =0°

3.2 Steady operational loads

In this section the consistency of the steady operational loads is verified between the two models. Both a standard upwind clockwise rotating rotor and a downwind anticlockwise rotor are included in the comparison.

3.2.1 Clockwise upwind rotor

The comparison in electrical power for the DTU rotor is given in Figure 3-4. The power difference results 0.6%-1.3% loss in energy capture compared to the old aerodynamics. When removing the blade flexibility this difference reduces to 0.4%-0.9%. Secondly the difference in power is reflected in the rotor speed signal (Figure 3-5) which shows a small difference as well.
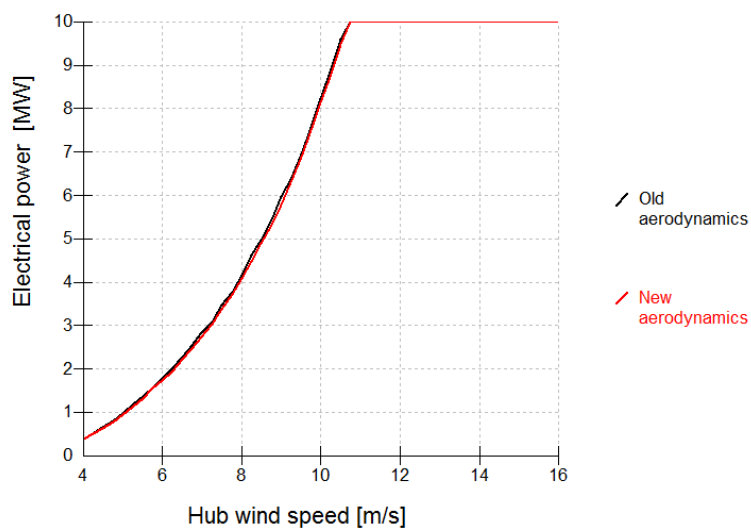

Figure 3-4 Comparison in steady operational electrical power, DTU rotor, flexibilities included
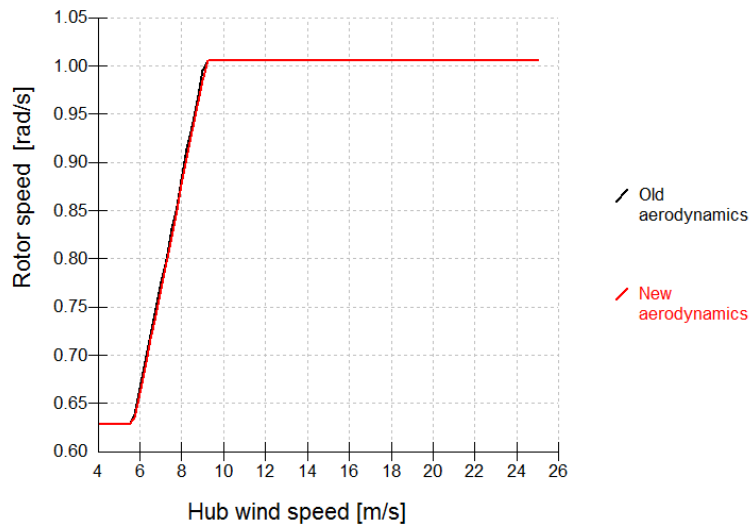
Figure 3-5 Comparison in steady operational rotor speed, DTU rotor, flexibilities included

Figure 3-6 to Figure 3-10 show the distributed inflow properties. As noted earlier in Section 3.1 there is a distinct difference between the old and new aerodynamics near the root (Figure 3-8). For 10m/s the differences in angle of attack are minor. Note however that removing the tilt and cone further reduces the differences between old and new aerodynamics. In old aerodynamics, the tilt angle is ignored in steady operational loads.

Figure 3-9 shows a difference in lift coefficient at the tip station. However, the applied aerodynamic load at the tip station equals zero in both the old and new aerodynamics, hence this does not influence the overall result.
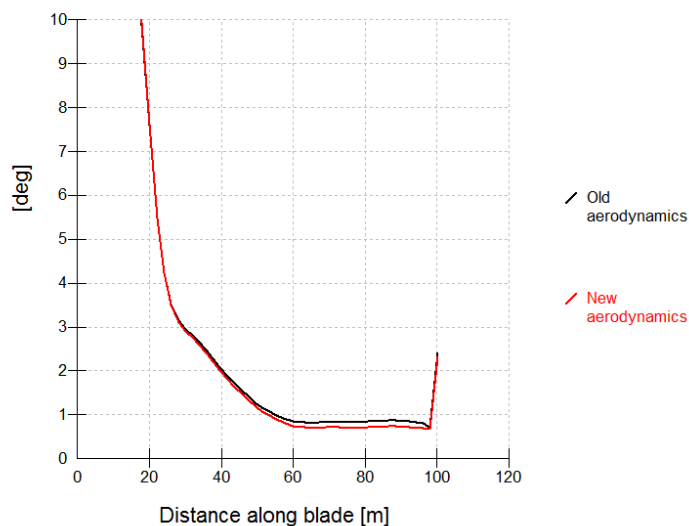

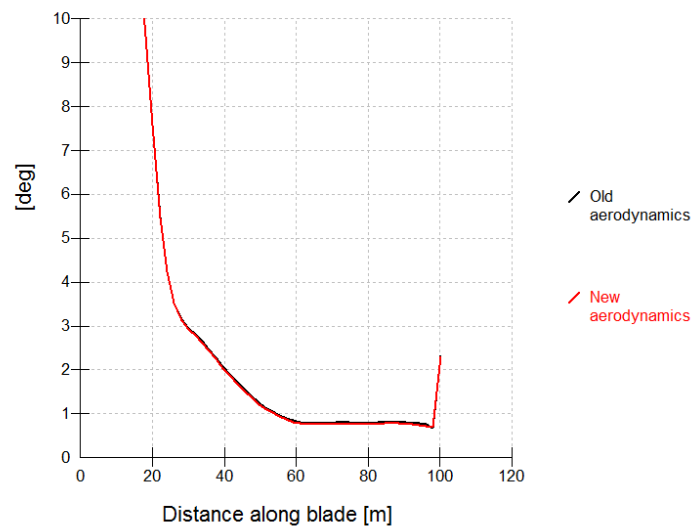**Figure 3-6 Comparison in angle of attack, DTU rotor, 10 m/s**

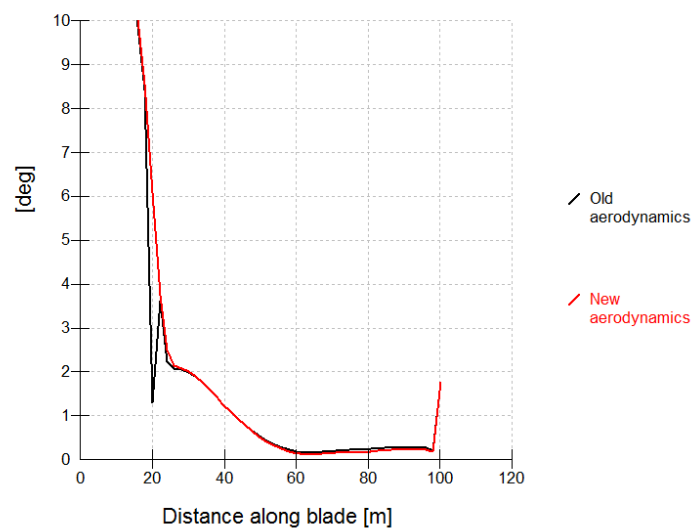**Figure 3-7 Comparison in angle of attack, DTU rotor, 10 m/s, no cone and tilt**

Figure 3-8 Comparison in angle of attack, DTU rotor, 8 m/s
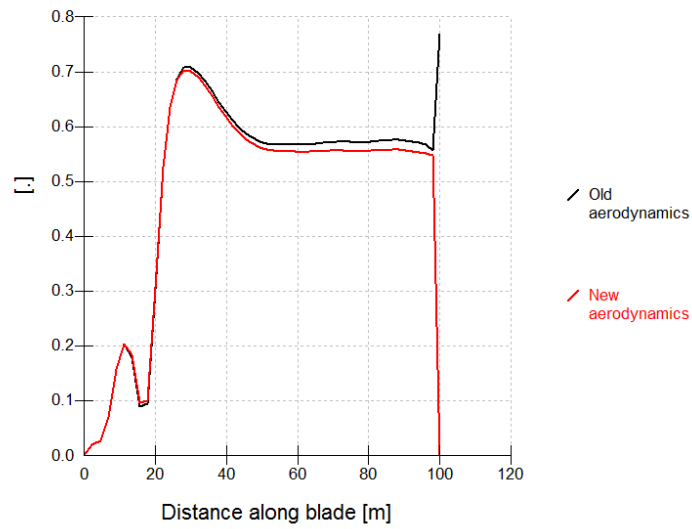
Figure 3-9 Comparison in lift coefficient, DTU rotor, 10 m/s
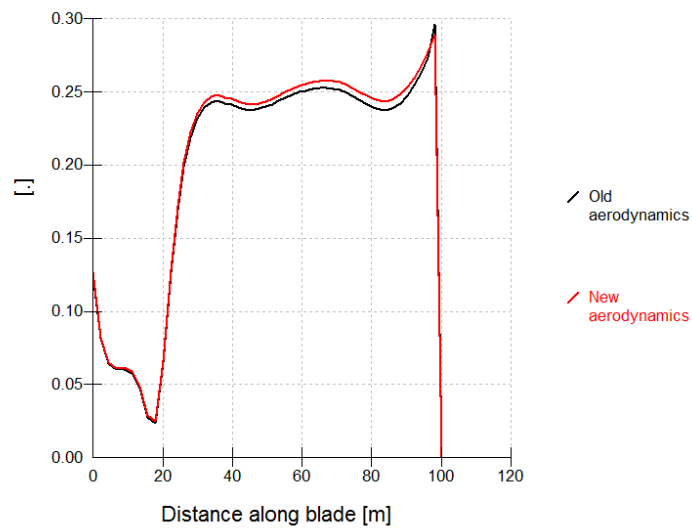

Figure 3-10 Comparison in axial induction factor, DTU rotor, 10 m/s

The blade torsional rotation and out of plane deflections shown in Figure 3-11 and Figure 3-12 match up well.
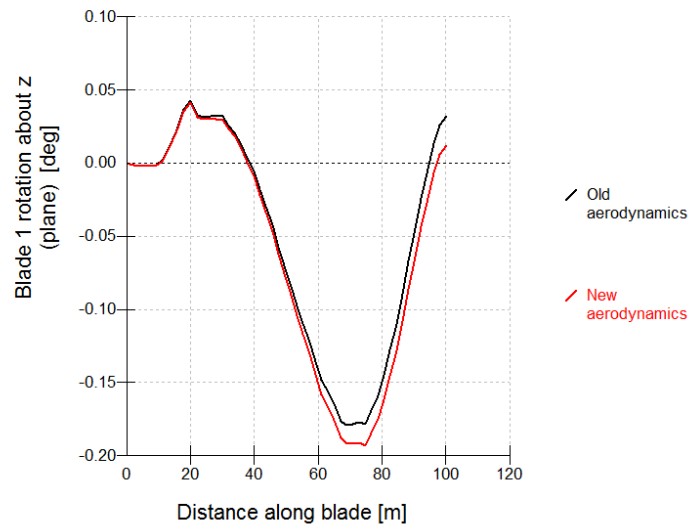
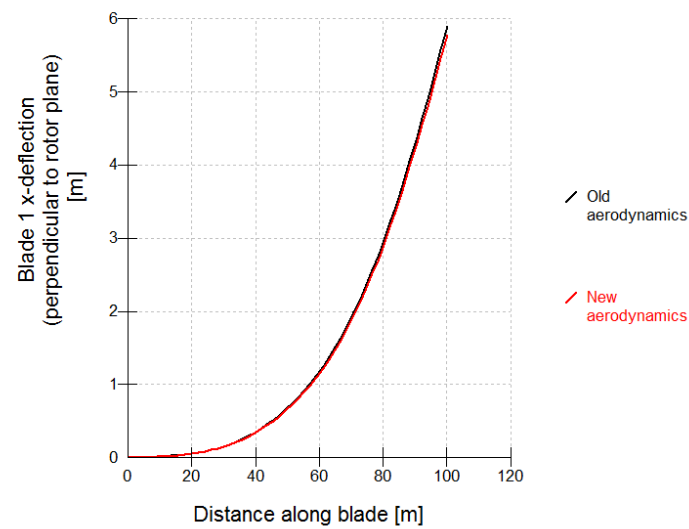**Figure 3-11 Comparison in blade torsional rotation, DTU rotor, 10 m/s**

Figure 3-12 Comparison in blade out of plane deflection, DTU rotor, 10 m/s

Further the rotor axial force and blade root pitching moment show good agreement in Figure 3-13 and Figure 3-14.
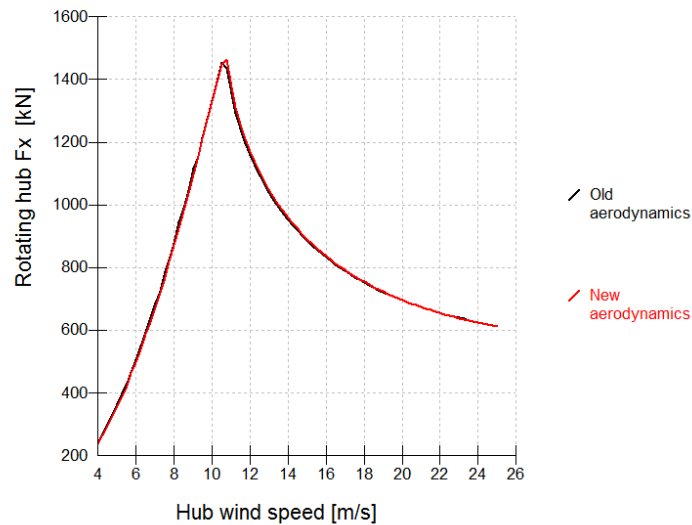
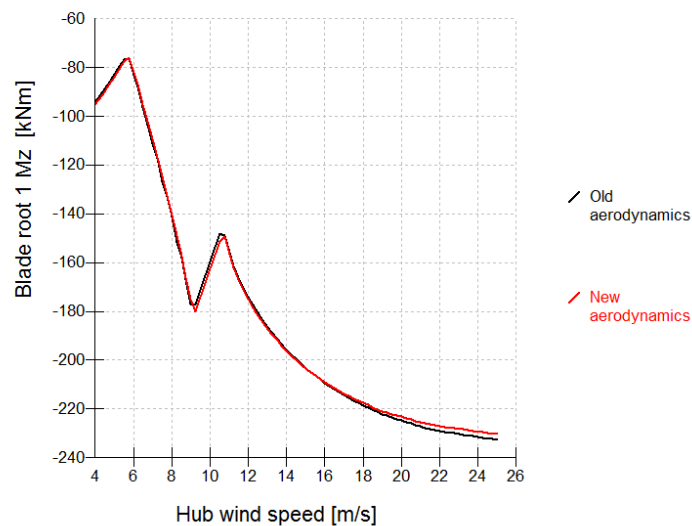**Figure 3-13 Comparison rotor axial force, DTU rotor**

Figure 3-14 Comparison in blade root pitching moment, DTU rotor

Some further notes must be made about the source of potential differences between the old and new aerodynamics:

- The old aerodynamics ignores tilt in steady operational load cases. The new aerodynamics however does not. Therefore, using a non-zero tilt angle will be a source of discrepancy.

- If the blade has a large degree of out of plane rotation due to (pre)bending, then this is accounted for in the mass flow calculation for the new aerodynamics. However, the old model will not take this effect into account. It is not expected that this will cause significant differences for common multi-MW wind turbines but could be of importance for passively controlled urban wind turbines that regulate power by bending the blade.

3.2.2 Anticlockwise downwind rotor

To verify the coordinate systems of the new aerodynamics, the steady operational loads are rerun for an anticlockwise downwind rotor. It is found from Figure 3-15 and Figure 3-16 that for this situation the loads are consistent in sign.
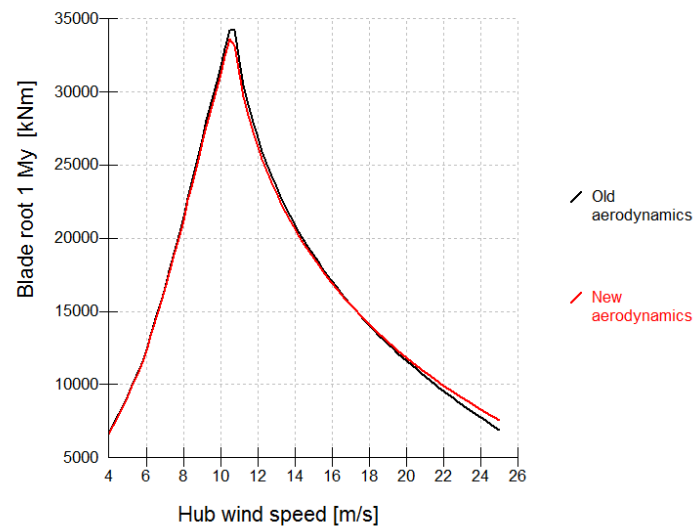
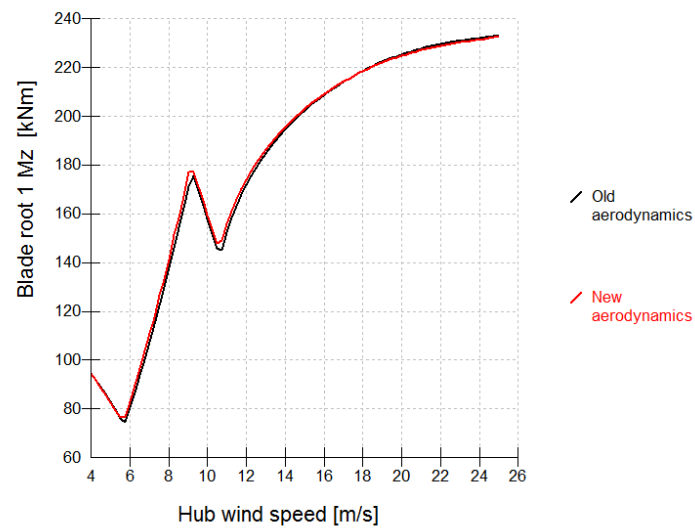**Figure 3-15 Comparison in steady blade root My downwind anticlockwise**

Figure 3-16 Comparison in steady blade root Mz downwind anticlockwise

4 VERIFICATION OF DYNAMIC MODELS

The implementation of the dynamic stall models is verified against analytical solutions and similar models in literature in a series of test cases. The theory behind the dynamic models can be found in the Bladed theory manual (ref /11/).

4.1 Dynamic stall

In order to test the dynamic stall models, the aerofoil is harmonically pitched such that the angle of attack is described as:

$$\alpha = \alpha_0 + \Delta\alpha \sin(\omega t)$$

In each test case, the steady state angle of attack α_0, the amplitude of oscillation $\Delta\alpha$, the Mach number M and the reduced frequency, k, given as:

$$k = \frac{\omega b}{U_\infty}$$

will be specified as an input to the new aerodynamics model.

4.1.1 Inviscid attached flow

In the Beddoes-Lieshman dyamic stall models the effect of shed vorticity on the local inflow conditions, which follows from the Theodorson theory, is approximated by the Wagner function. This function describes the lift reponse of a flat-plate aerofoil due to a step in angle of attack.

As an initial test, the model is given a step change in angle of attack of 5°, such that the angle of attack is given by:

$$\alpha = \begin{cases} 0° & \tau \leq 0 \\ 5° & \tau > 0 \end{cases}$$

The Mach number in this case was $M = 0.379$. The result of the simulation is compared against the approximation of Wagner's indicial lift function as given in reference /2/.

$$\varphi(\tau) = 1 - 0.165e^{-0.0455\tau} - 0.355e^{-0.3\tau}$$

$$\Delta C_l(\tau) = C_{l\alpha} \cdot \varphi(\tau) \tag{4.1}$$

$$\tau = \frac{2U_\infty t}{c}$$

Figure 4-1 shows that the computed indicial response function matches well to the analytic solution.
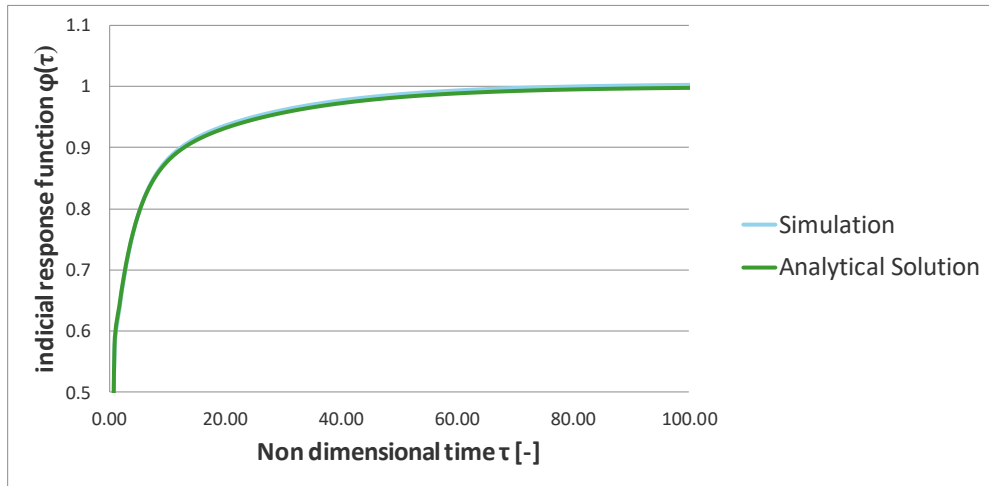
Figure 4-1 Comparison of analytical and simulation for a step change of 5 degrees, flat-plate aerofoil

In the second test, the dynamic solution is compared against the Theodorson analytical solution (see Ref /1/) for a harmonically pitching aerofoil.

$$L = \pi \rho b^2 U_\infty \dot{\alpha} + 2\pi \rho U_\infty b C(k)[U_\infty \alpha + b/2 \dot{\alpha}]$$

$$M_{(0.25c)} = -\pi \rho b^3 U_\infty \dot{\alpha}$$

4.2

$$k = \frac{\omega b}{U_\infty}$$

Where:
- b, semi-chord length
- U_∞, local wind speed
- $C(k)$, Theodorson function
- α, angle of attack
- $\dot{\alpha}$, rate of change of angle of attack
- ω, angular frequency of oscillation
- k, reduced frequency

Figure 4-2 illustrates that this oscillating aerofoil simulation reproduces the analytical solution with sufficient accuracy.
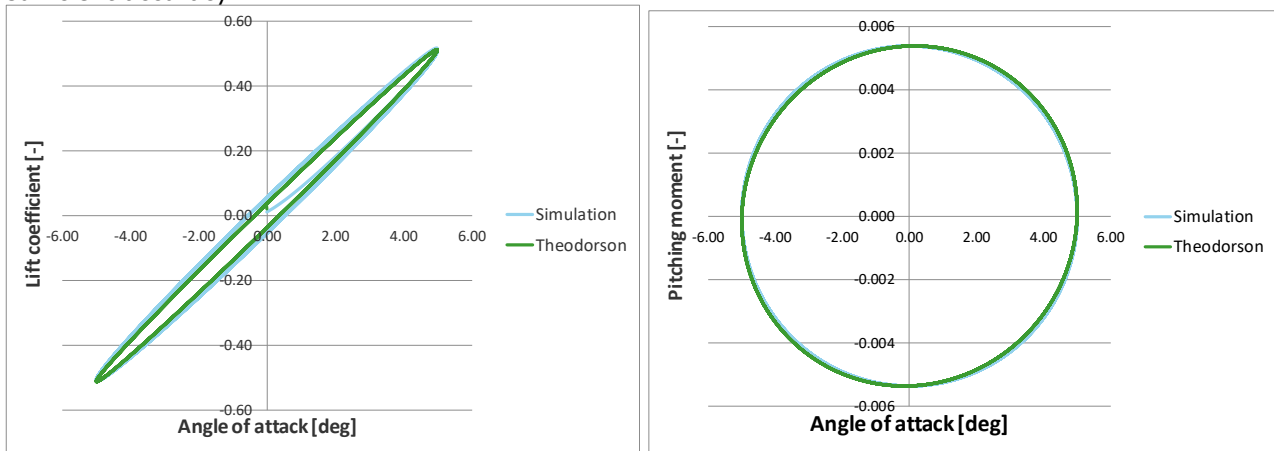

Figure 4-2 Unsteady lift and moment coefficient for harmonically pitching flat-plate aerofoil, (reduced frequency = 0.0393, Δα=5)

4.1.2 Impulsive lift terms in compressible model

The numerical state-space equations for impulsive lift and moment terms due to step changes in angle of attack and pitch rate are tested against their analytical solutions. The analytical equations can be found in Ref /1/.

The following results are obtained for the normal force coefficient (C_n) and the pitching moment coefficient (C_m):
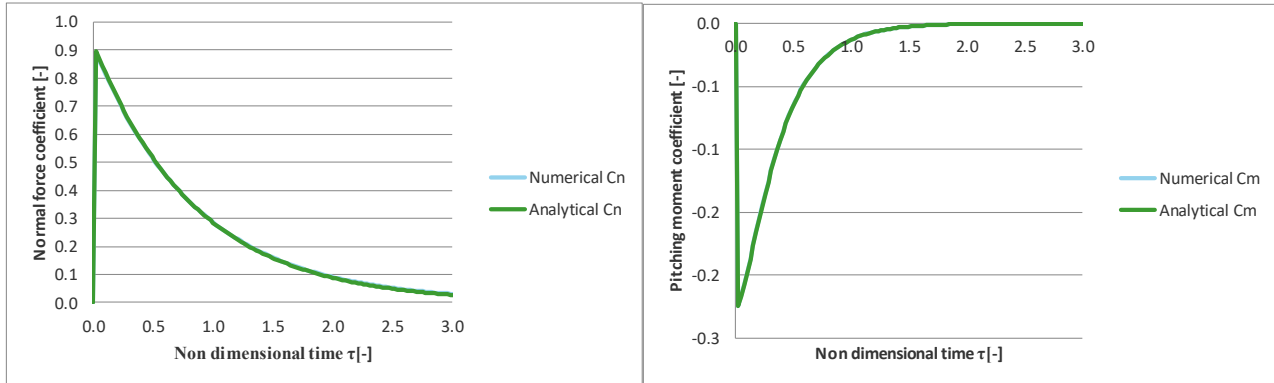

Figure 4-3 Comparison of numerical vs. analytical normal force and pitching moment coefficients due to a step change in angle of attack of 5º.

Figure 4-3 shows that the numerical and analytical solution match exactly. It is found though that the accuracy of the numerical integration is strongly dependent on the time step used. By nature, the impulsive lift effects decay rapidly requiring a sufficiently small time step.

For a step change in non-dimensional pitch rate $q = \frac{d\alpha}{dt}\frac{c}{V} = 0.135$, with Mach number $M = 0.379$, the following results are obtained:

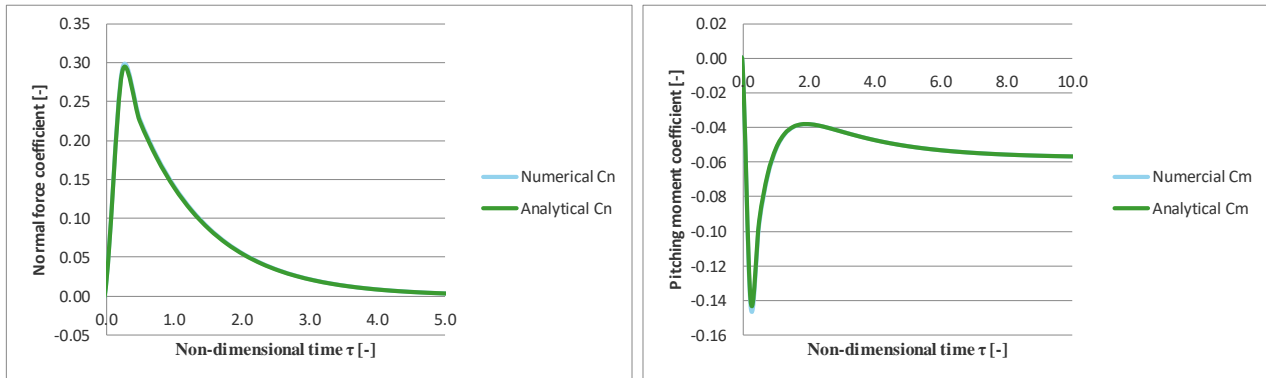**Figure 4-4 Comparison of numerical vs. analytical normal force and pitching moment coefficients following a step change in pitch rate of $q = 0.135$.**

A good agreement is found between the analytical and numerical solutions. Note that the pitching moment coefficient value eventually settles to the circulatory term of the moment coefficient:

$$C_m = -\frac{\pi \beta b_5 T_u \dot{\alpha}}{4}$$

4.3

4.1.3 Comparison against Beddoes-Leishman predictions using NACA0012 aerofoil

The Bladed compressible and incompressible Beddoes-Leishman dynamic stall models were compared against data from the NACA0012 aerofoil. This test data, which is shown on the left-hand side of each figure is a comparison between the Beddoes-Leishman dynamic stall models and measured data in a study originally done by Leishman, which is documented in reference /2/. Against this reference, three Bladed dynamic stall models in the new aerodynamics were compared:

- Compressible Beddoes-Leishman without impulsive lift and moment contributions

- Compressible Beddoes-Leishman with impulsive lift and moment contributions

- Incompressible Beddoes-Leishman without impulsive lift and moment contributions

The following values of the time constants are used, which are all the default or hard-coded Bladed values:

$$T_f = 3.0 \text{ (separation position time constant)}$$
$$T_p = 1.7 \text{ (pressure lag time constant)}$$
$$T_v = 6.0 \text{ (vortex lift time constant)}$$

$$T_{vl} = 7.5 \quad A_1 = 0.3 \quad A_2 = 0.7 \quad b_1 = 0.14 \quad b_2 = 0.53 \quad A_3 = 0.15 \quad A_4 = -0.5 \quad b_3 = 0.25 \quad b_4 = 0.1$$

As determined by the original experiment on the NACA0012 aerofoil data, the aerofoil is pitched sinusoidally such that:

$$\alpha_0 = 10.3, \quad \Delta\alpha = 8.1, \quad k = 0.075, \quad M = 0.379$$

The compressible and incompressible models reproduce the Beddoes-Leishman normal force coefficient well. The underside of the hysteresis loop is smaller however (near points 3 and 4 in Figure 4-5). This difference is likely explained by the absence of a reattachment delay in the Bladed implementation.

Figure 4-5 Comparison of normal force coefficient in three Bladed dynamic stall models against original NACA0012 measured and simulated data.

The asymmetric moment coefficients are captured well and match the hysteresis loop shown in Figure 4-6. The vortex lift contribution here shows a significant importance as when the detached vortex reaches the trailing edge the minimum pitching moment coefficient (C_m) value is reached.

Figure 4-6 Comparison of pitching moment in three Bladed dynamic stall models against original NACA0012 measured and simulated data.

The difference in drag coefficient is most noticeable. A possible reason for the deviation could be caused by a mismatch in the underlying steady drag coefficient data. The data used in the Bladed simulations is based on RFOIL calculations using free transition and a Reynolds number of 10^6. It is unknown which data is used exactly in the original Leishman model.
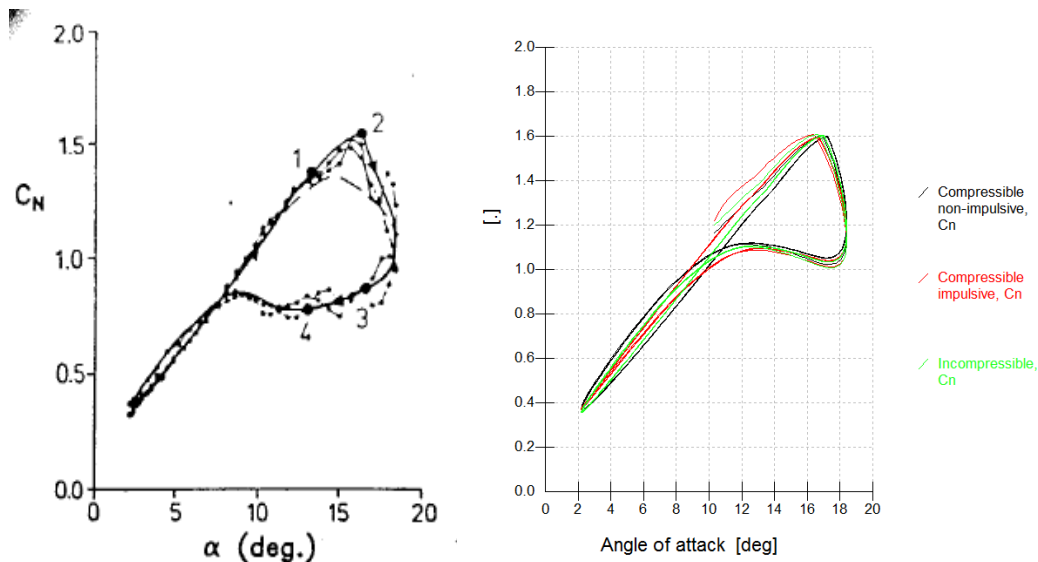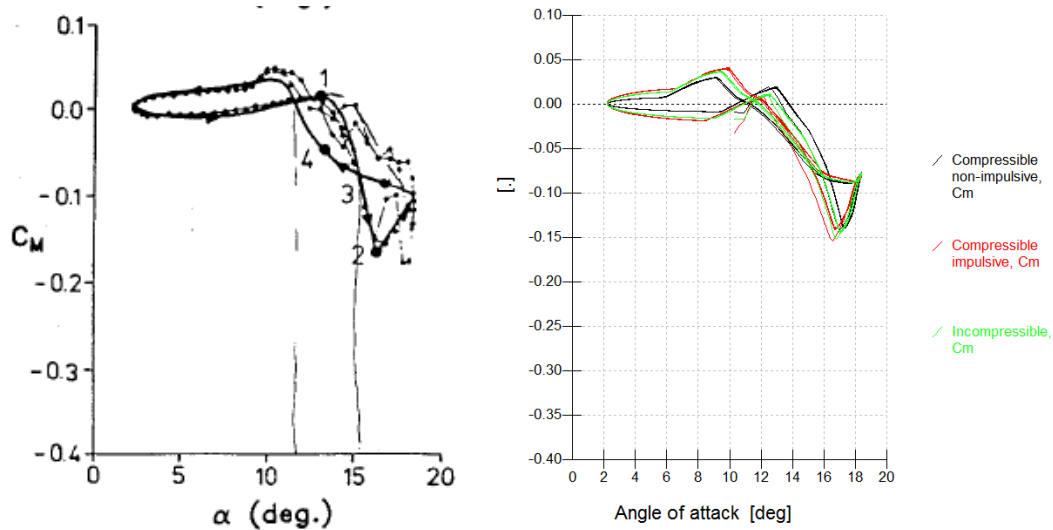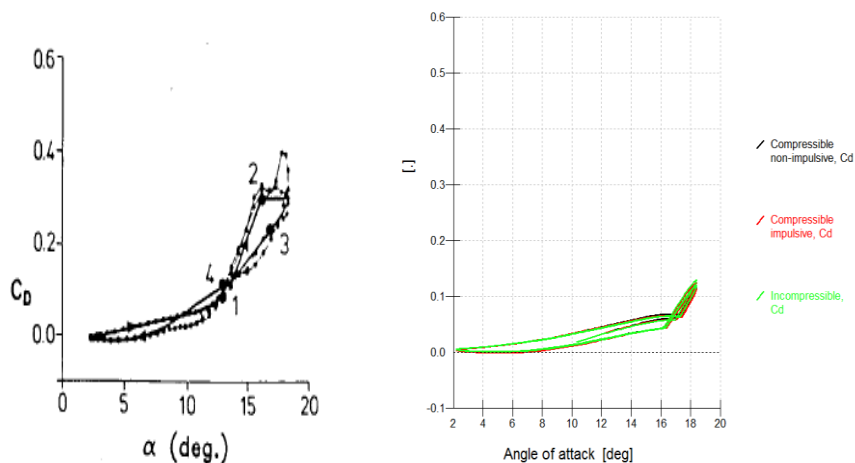

Figure 4-7 Comparison of drag coefficient in three Bladed dynamic stall models against original NACA0012 measured and simulated data.

Additionally, comparisons were done for an attached flow case, where the aerofoil does not go into deep stall. In this case, the aerofoil was pitched sinusoidally such that:

$$\alpha_0 = 2.1°, \quad \Delta\alpha = 8.2°, \quad k = 0.074, \quad M = 0.383$$

Figure 4-8 to Figure 4-10 show that there is a good comparison for the attached flow simulations. The Bladed simulations do however show a bit of vortex contribution in the moment coefficient which is not found in the original simulations. Furthermore, the moment coefficient in the original Leishman data shows a dent in the loop near zero degree angles of attack. Finally, the shape in drag coefficient matches well albeit that the Bladed simulations show a positive offset of the loop.
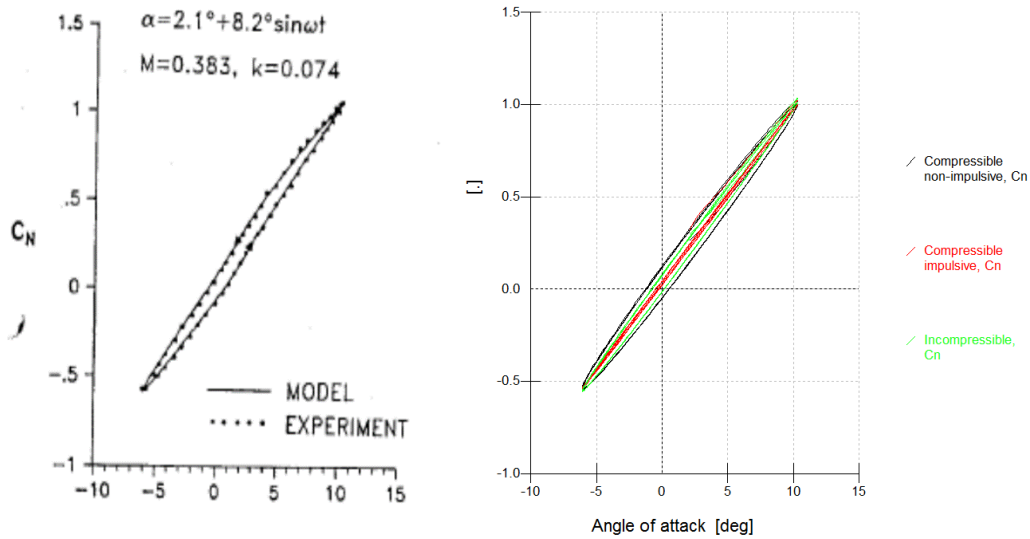
Figure 4-8 Comparison of normal force coefficient in three Bladed dynamic stall models against original NACA0012 measured and simulated data in attached flow.

Figure 4-9 Comparison of pitching moment coefficient in three Bladed dynamic stall models against original NACA0012 measured and simulated data in attached flow.

Figure 4-10 Comparison of drag coefficient in three Bladed dynamic stall models against original NACA0012 measured and simulated data in attached flow.

Finally, the aerofoil was pitched sinusoidally in the region where vortex lift hysteresis is exhibited. In this case:

$$\alpha_0 = 5.2°, \qquad \Delta\alpha = 8.4°, \qquad k = 0.074, \qquad M = 0.381$$

Figure 4-11 to Figure 4-13 show that for the normal force coefficient, the vortex lift hysteresis is not captured. In the Bladed simulations, the vortex lift term is not yet triggered i.e. the critical normal force

coefficient has not been reached. Increasing the amplitude of the oscillation to 10.4° does show vortex shedding in the normal force coefficient. (see Figure 4-14)

Figure 4-11 Comparison of normal force coefficient in three Bladed dynamic stall models against original NACA0012 measured and simulated data around the vortex lift point.

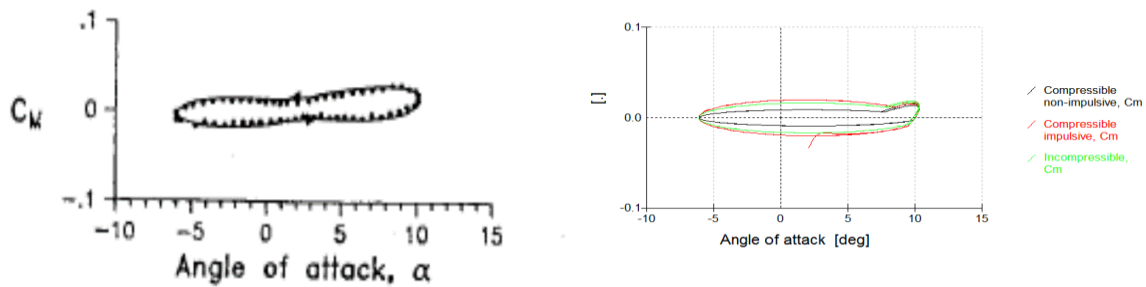**Figure 4-12 Comparison of pitching moment coefficient in three Bladed dynamic stall models against original NACA0012 measured and simulated data around the vortex lift point.**
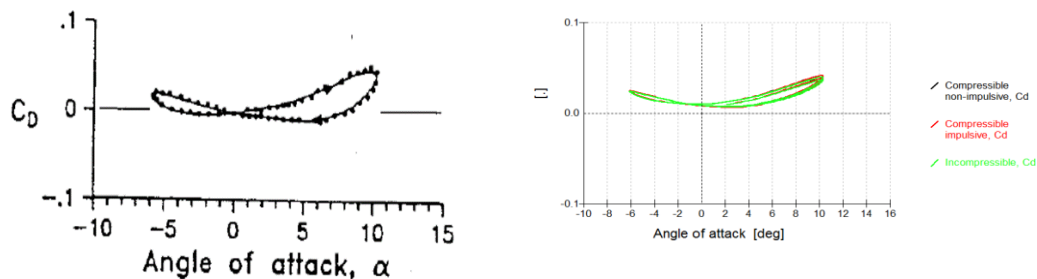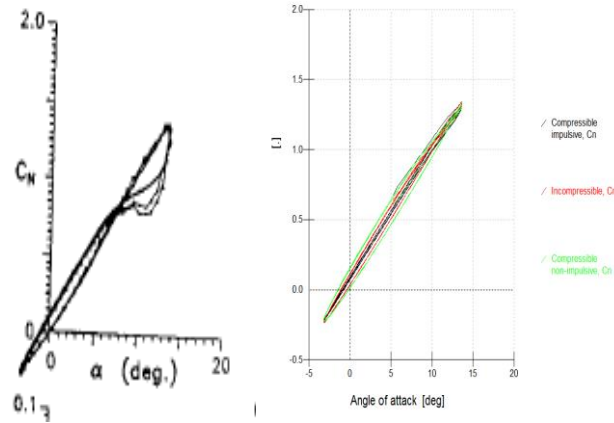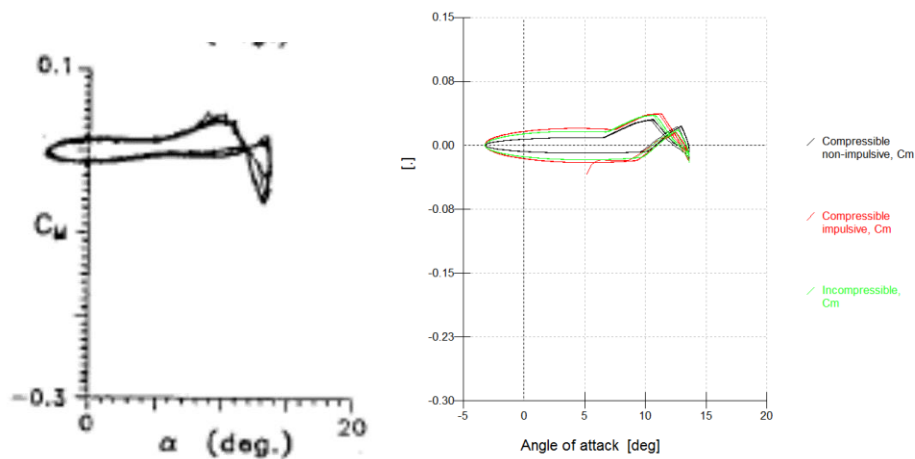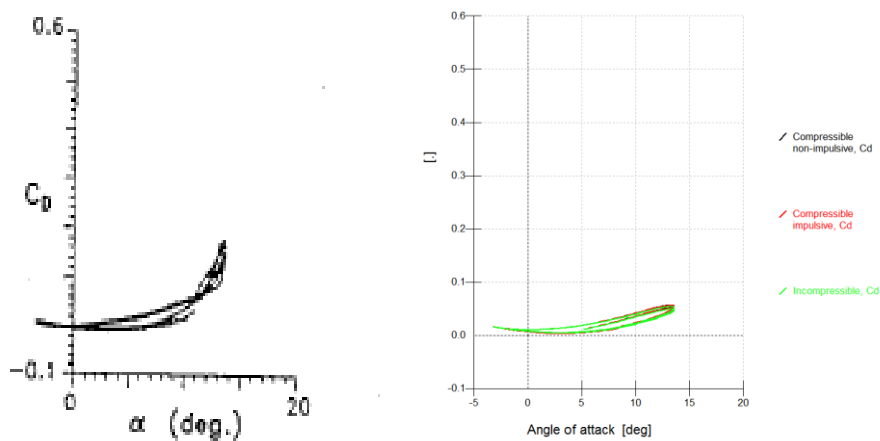

Figure 4-13. Comparison of drag coefficient, in three Bladed dynamic stall models against original NACA0012 measured and simulated data around the vortex lift point.
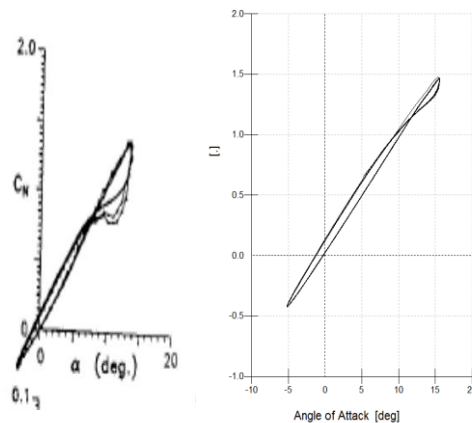
Figure 4-14 same as Figure 4-11, Simulation uses amplitude of $\Delta\alpha = 10.4°$.

4.1.4 Verification of implementation of pre-4.8 Beddoes-Leishman model in new aerodynamics

As described in the theory manual Ref. /11/ the dynamic stall models implemented in the new aerodynamics module are not exactly equal to the model implemented in the pre-4.8 Bladed aerodynamics. To provide backward compatibility of the results the implementation of pre-4.8 Beddoes-Leishman model is also carried forward into the new aerodynamics. This section describes the results of the verification that is carried out for this new model.

Figure 4-15 to Figure 4-17 shows the comparison in lift, drag and moment coefficient between the old aerodynamics (in Bladed 4.7) and the new aerodynamics with the pre-4.8 Beddoes-Leishman model implemented. The following is observed:

- A difference is found in peak lift coefficient. It is found that an error in the old aerodynamics causes the vortex lift to accumulate for a too short time period.

- At low angles of attack the pitching moments in old aerodynamics are larger. It is found that there is an error in the impulsive contribution of the pitching moment which does not match the analytical solution presented in Figure 4-3. The additional line in Figure 4-17 shows the result when this error is corrected in the old aerodynamics.

Figure 4-15, lift coefficient comparison between Old aerodynamics, and old-style Beddoes Leishman, NACA0012, k=0.075, Δα=8.1, α$_0$=10.3, M=0.379
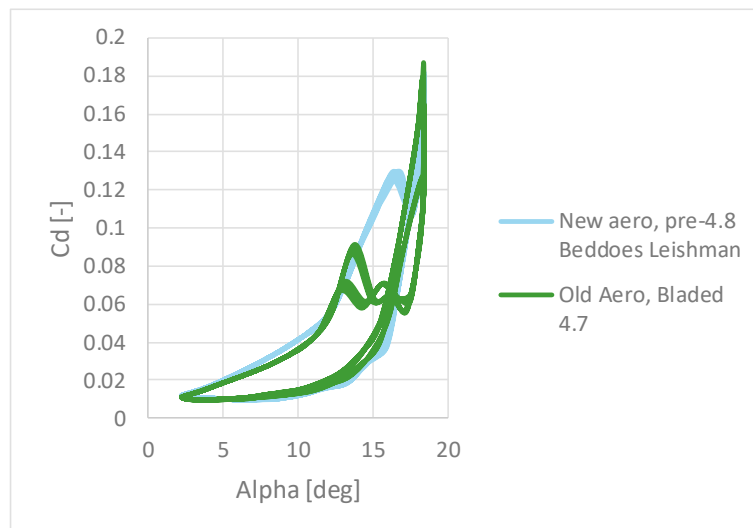
Figure 4-16, drag coefficient comparison between Old aerodynamics, and old-style Beddoes Leishman, NACA0012, k=0.075, Δα=8.1, α$_0$=10.3, M=0.379
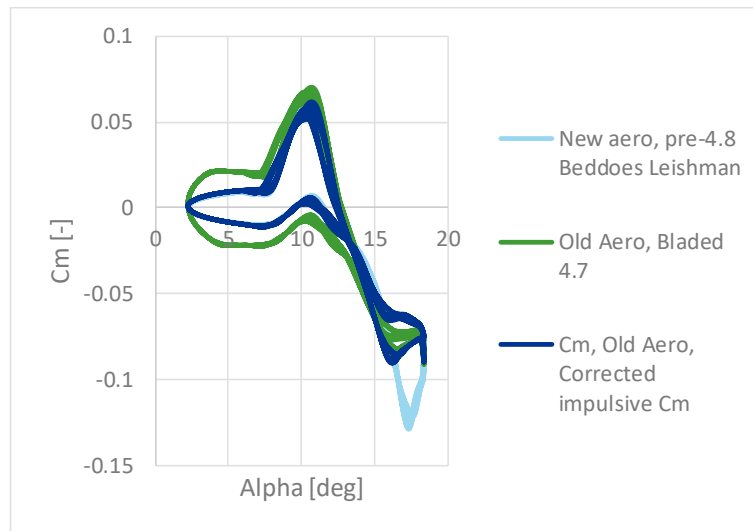
Figure 4-17, moment coefficient comparison between Old aerodynamics, and old-style Beddoes Leishman, NACA0012, k=0.075, Δα=8.1, α$_0$=10.3, M=0.379

Figure 4-18 to Figure 4-20 show a similar comparison for a mean angle of attack of 2.1°. For these conditions there is no vortex lift contribution. As a result the lift and drag coefficient are identical. The moment coefficient is matching as well in case the impulsive lift contribution in the old aerodynamics is corrected.
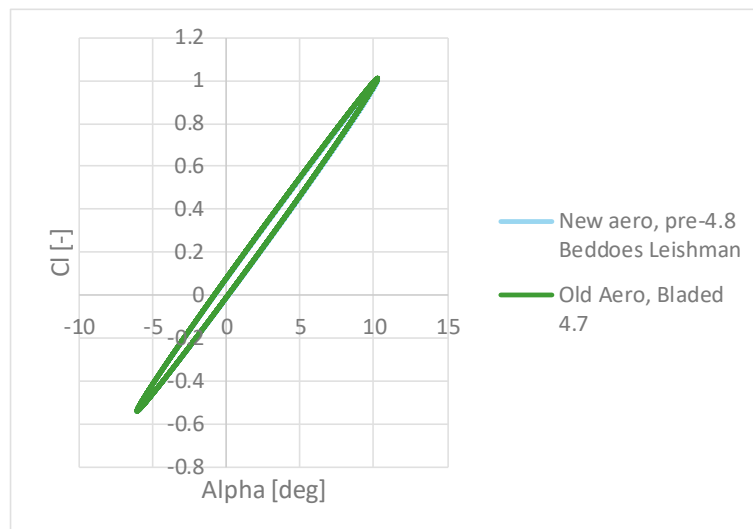
Figure 4-18, lift coefficient comparison between Old aerodynamics, and old-style Beddoes Leishman, NACA0012, k=0.074, Δα=8.2, α$_0$=2.1, M=0.383
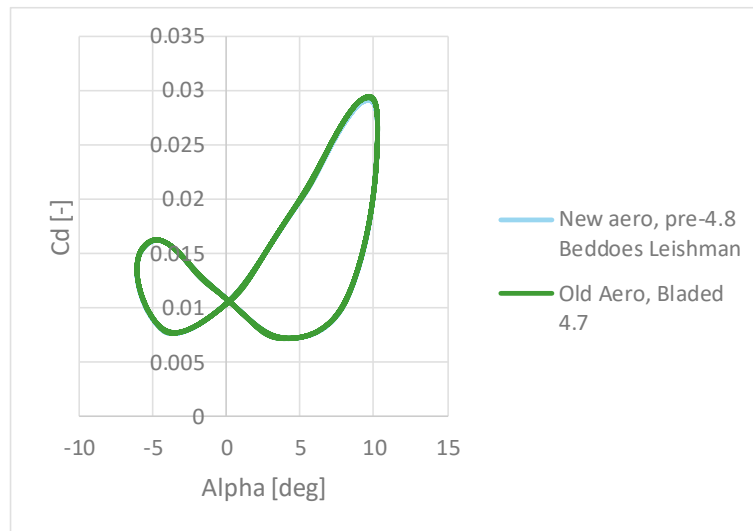
Figure 4-19, drag coefficient comparison between Old aerodynamics, and old-style Beddoes Leishman, NACA0012, k=0.074, Δα=8.2, α$_0$=2.1, M=0.383
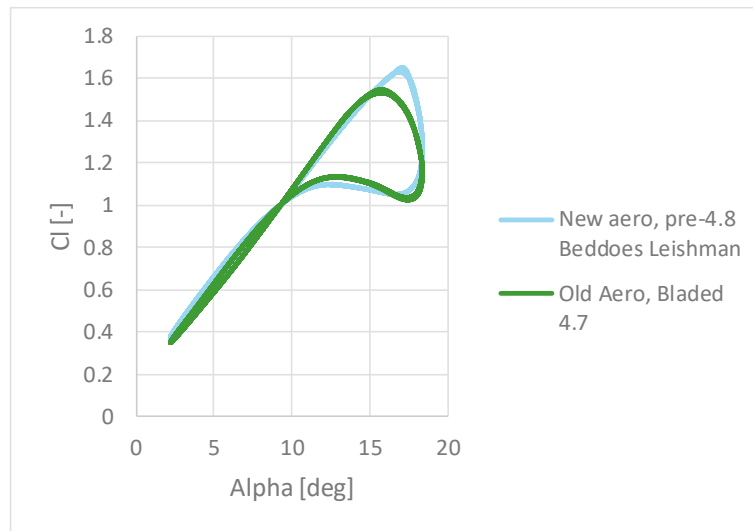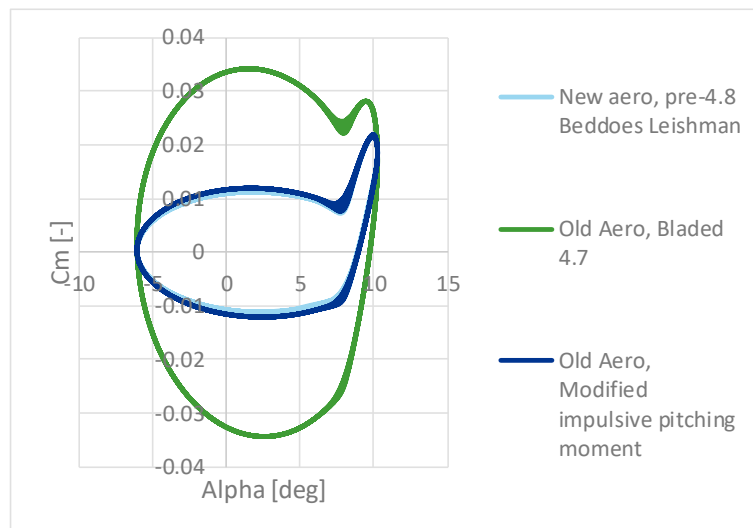

Figure 4-20, moment coefficient comparison between Old aerodynamics, and old-style Beddoes Leishman, NACA0012, k=0.074, Δα=8.2, α$_0$=2.1, M=0.383

Finally, the models are compared for a deep-stall scenario using a NACA64618 aerofoil. The lift, drag and pitching moment coefficients match up well.
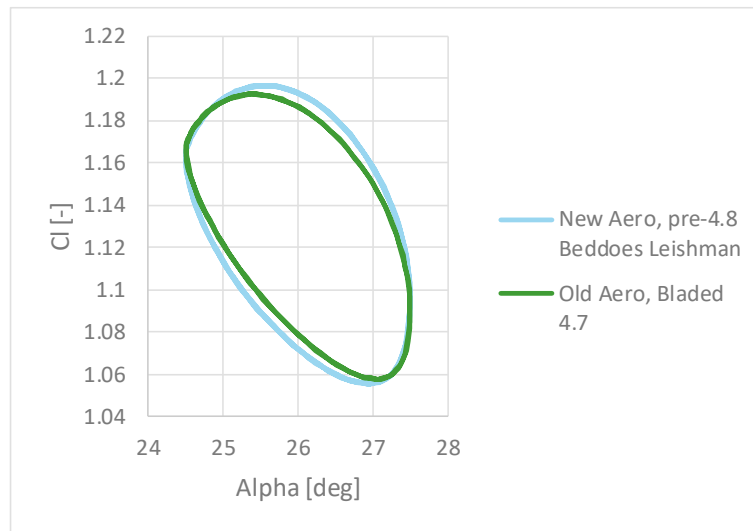
Figure 4-21, lift coefficient comparison between Old aerodynamics, and old-style Beddoes Leishman, NACA64618, $\alpha = 26° + 1.5°sin(1.257\pi t), V_\infty = 50m/s,$
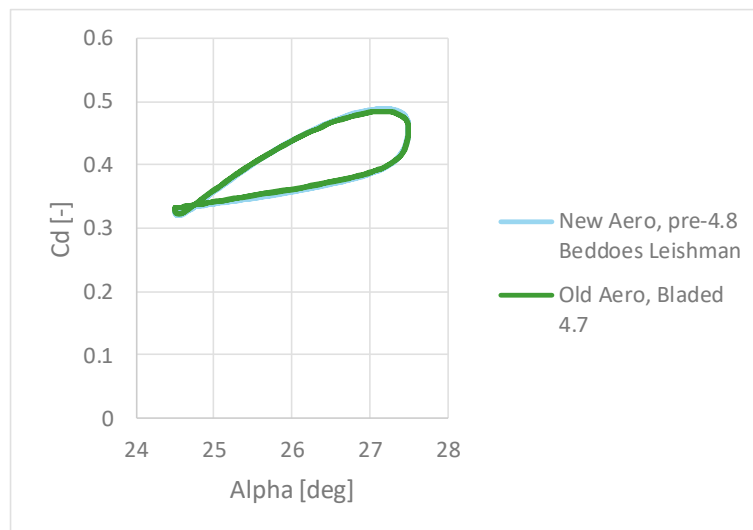
Figure 4-22, drag coefficient comparison between Old aerodynamics, and old-style Beddoes Leishman, NACA64618, $\alpha = 26° + 1.5°sin(1.257\pi t), V_\infty = 50m/s$
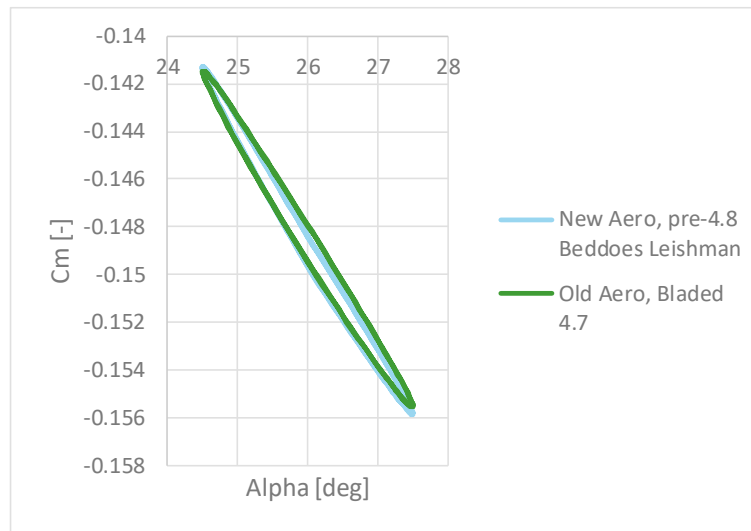
Figure 4-23, moment coefficient comparison between Old aerodynamics, and old–style Beddoes Leishman, NACA64618, $\alpha = 26° + 1.5°sin(1.257\pi t), V_\infty = 50m/s$

4.1.5 Reconstruction of original aerofoil data

In the steady state case, the dynamic stall model should return the stationary lift, drag and moment coefficient data. This was tested in two different ways:

- The angle of attack was varied from -180° to +180° and for each angle a steady solution is calculated for the aerodynamic states.

- A dynamic simulation was carried out where the aerofoil oscillates in pitch at 0.0025 Hz. This slow oscillation should then cause all the dynamic states to decay and return the steady aerofoil data.
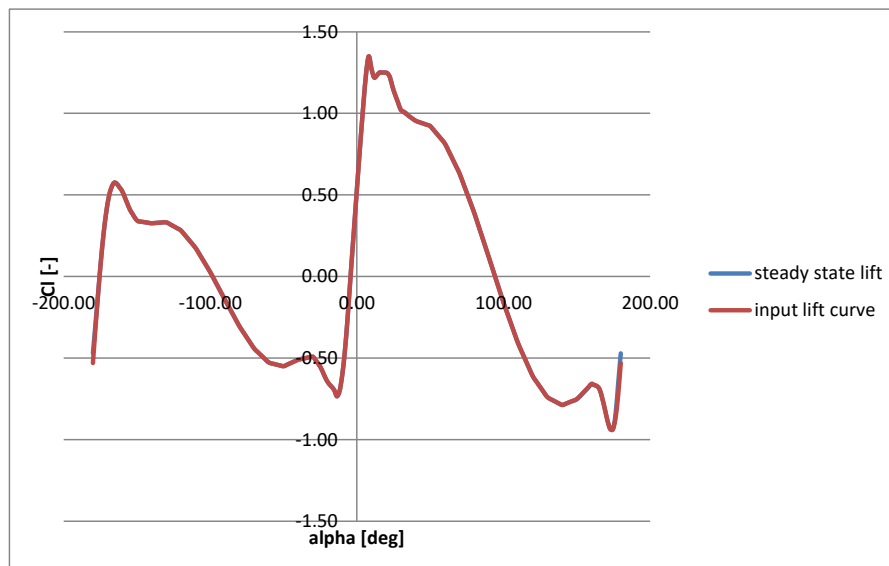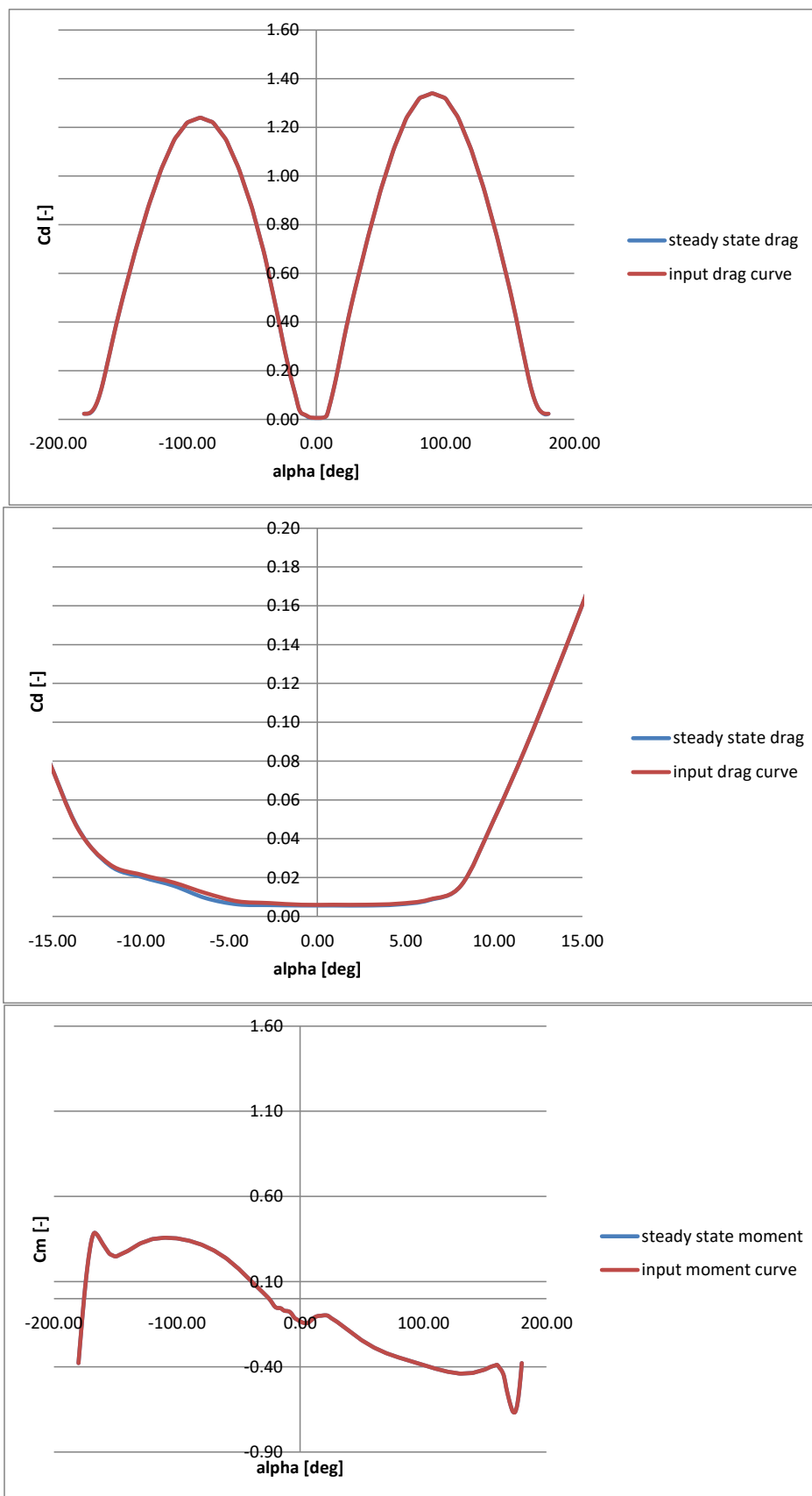
Figure 4-24. Reconstruction of steady state aerofoil coefficients

As shown in Figure 4-24, the aerodynamic coefficients are reproduced well with the steady calculation, aside from some local deviations.

Dynamic simulations with a low frequency oscillation of angle of attack were performed with:

$$\alpha = -15 + 30 \sin\left(\frac{2\pi}{400}t\right)$$
$$M = 0.25$$
$$k = 9 \times 10^{-4}$$

This corresponds to a frequency of 0.0025Hz.
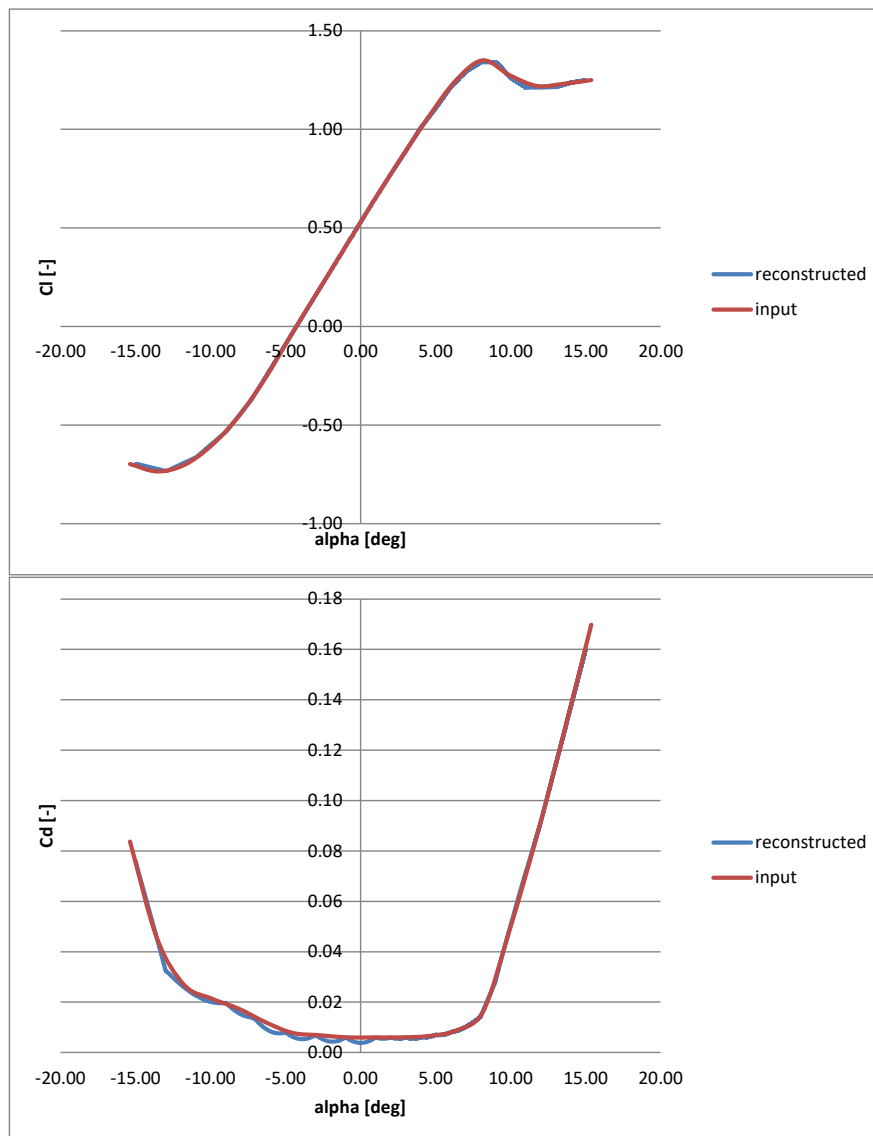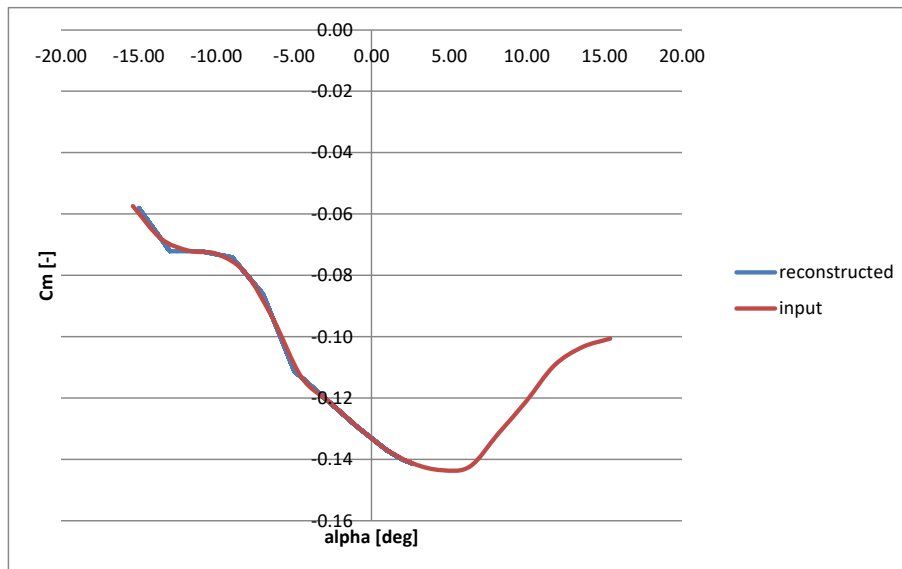
Figure 4-25 Reconstruction of aerofoil data with dynamic simulation using a low frequency variation in angle of attack.

In the dynamic case with a very low frequency, the steady lift curves are reproduced quite well as shown in Figure 4-25. It must be noted however that for a proper reconstruction of the drag coefficient, a step size no larger than 0.5° angle of attack is recommended in the lift and drag coefficient lookup tables.

4.1.6   Backwinded flow

A challenging case for the dynamic stall models is the backwinded flow situation, especially when the angle of attack is switching between +/-180 degrees continuously. In this case, the angle of attack was given by:

$$\alpha = -179 + 5sin(4\pi t)$$
$$M = 0.25$$

Figure 4-26 shows that the code can deal with the backwinded flow case satisfactorily.
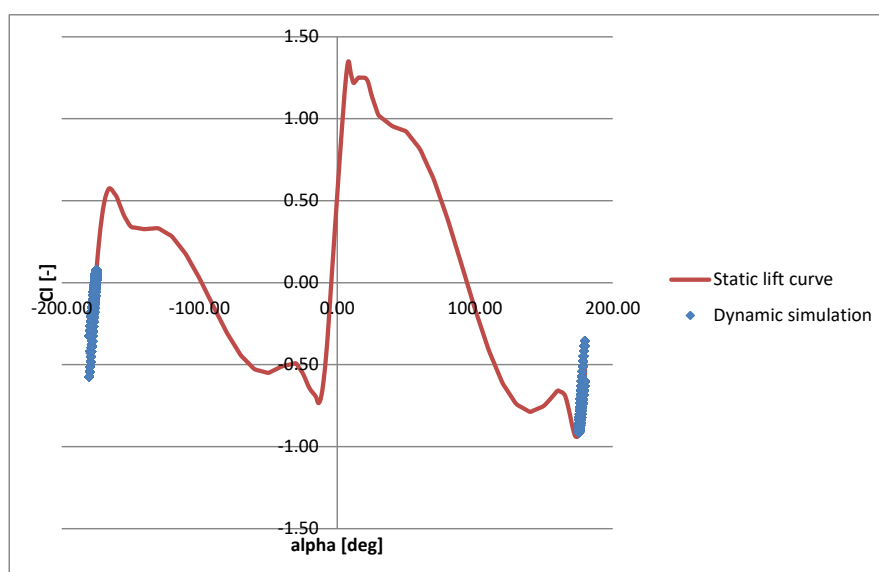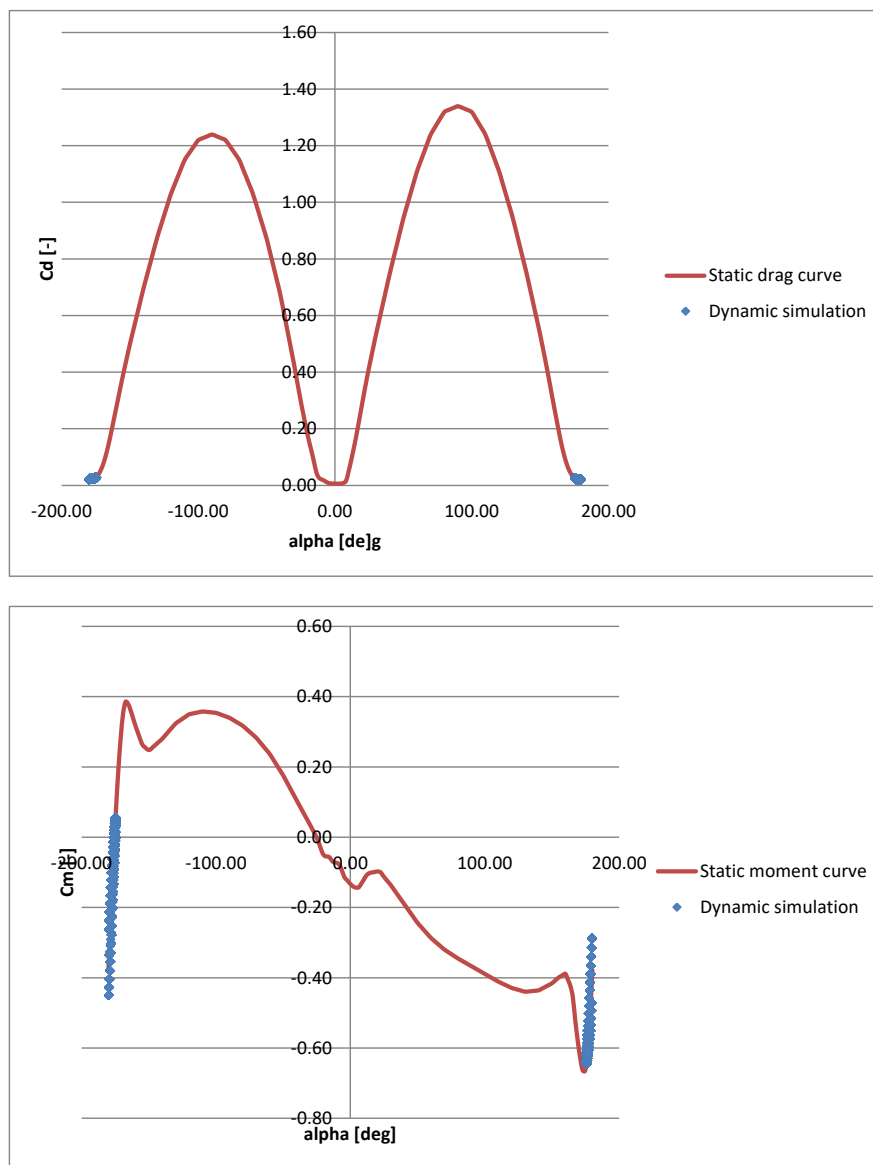
Figure 4-26. Reproduction of aerofoil data in a dynamic simulation in a backwinded case

4.2 Verification of dynamic wake models

As a verification step of the dynamic wake models, the well-known Tjaereborg pitch-step case is reproduced /8/. The following observations can be made:

- The old aerodynamics code shows the most rapid recovery.

- The Pitt & Peters model in the new aerodynamics shows a somewhat slower recovery than the Pitt & Peters model in the old aerodynamics code. This is due to the different interpretation of the added mass constant.

- A comparison of the calculations and the measurements shows that the Øye dynamic wake model provides the best replication on the measurements. This finding is also supported in [/7/].
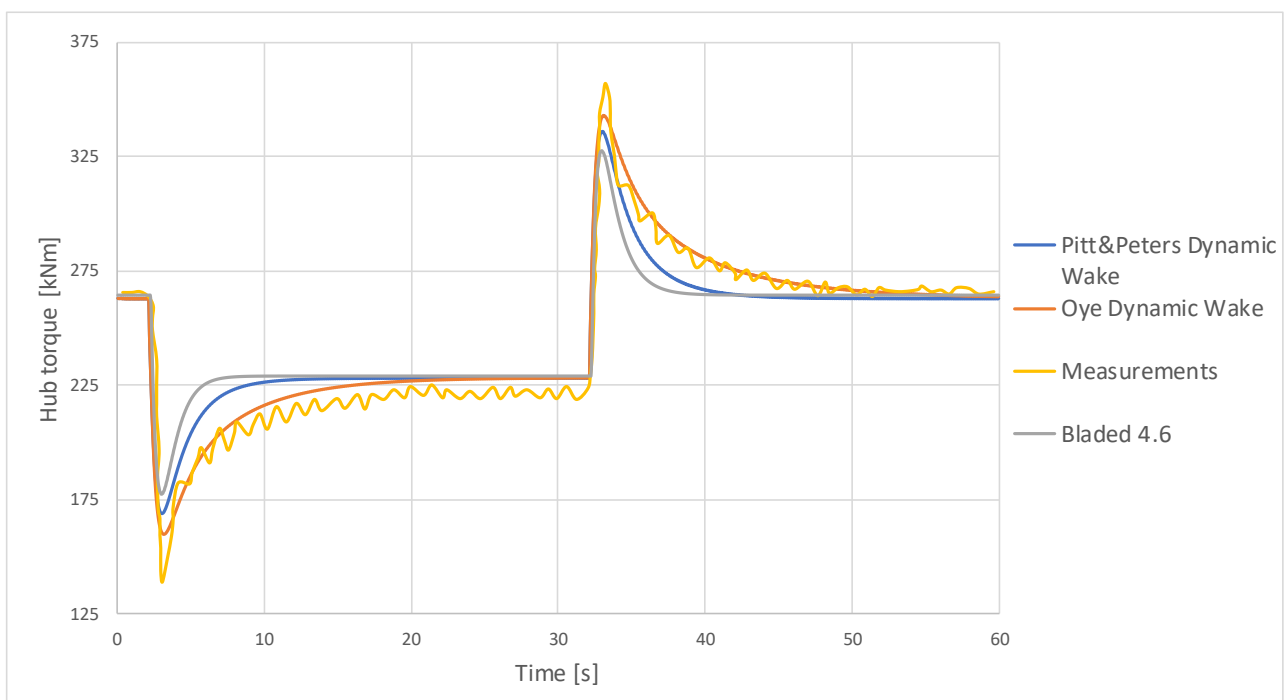
Figure 4-27. Bladed BEM code pitch step case with three different models compared against Tjaereborg measurements

To match the initial shaft torque of the mesurements the wind used in the Bladed simulations was increased to 9 m/s. The measurements however report a wind speed of 8.7 m/s.

5 SIMULATION OF THE NREL PHASE VI TURBINE

DNV GL is part of the MexNext consortium. During the MextNext project a blind comparison between codes of different project partners and the Nasa-Ames measurements has been conducted. The full results, including a comparison of Bladed against other codes can be found in the MexNext final report (reference /14/).

This chapter contains a summary of the comparison between Bladed and two test cases. The primary difference between the cases is that one rotor is lightly yawed away from the flow while the second is heavily yawed from the flow.

5.1 Case description

For the second round of MexNext II project calculations a closer look is taken at the NREL phase VI rotor experiment. A detailed description of the rotor and experimental set up can be found in /3/. The following table describes the two cases that are considered:

Case	V_{tunnel} [m/s]	Pitch angle [deg]	Rotational speed [rpm]	Yaw angle [deg]	ρ [kg/m^3]	p_{inf} [N/m^2]
2.1 (X05M0101)	4.997	2.98	90.19	10.127	1.2253	101517
2.2 (X05M0301)	4.994	2.99	90.18	29.9840	1.2252	101508

Figure 5-1 case description

Local flow variables and forces are requested to be calculated at 30%, 47%, 63%, 80% and 95% of the local blade radius measured from the hub centre. Furthermore, the integral aerodynamic torque and axial force are calculated.

5.2 Turbine model

The input of the turbine geometry is provided by the MexNext consortium to ensure consistency between the participants. Details of the model can also be found in /3/
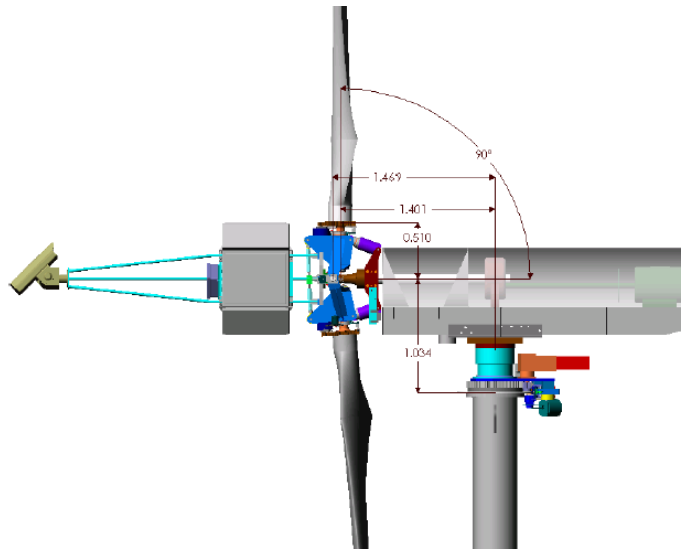
Figure 5-2. sketch of Phase VI rotor

5.3 Aerodynamic model

Both the current and new Bladed BEM codes are used in the calculations. Furthermore, the results are compared against a vortex lifting line code developed as a beta version within Bladed. The latter code is expected to provide more accurate results in yawed flow conditions, compared with BEM. Details on the vortex line model are documented in /4/.

For the old Bladed aerodynamics model, the following settings are used:

- Pitt & Peters Dynamic wake

- Compressible Beddoes-Leishman dynamic stall

- Axial momentum theory without skew-wake correction

For the new aerodynamics module in Bladed, the following settings are used:

- Øye Dynamic wake

- Incompressible Beddoes-Leishman dynamic stall

- Glauert momentum theory combined with a skew-wake correction

Finally, the vortex lifting line code uses no dynamic stall model. However, the dynamic wake of the vortex line method will inherently provide some attached flow hysteresis due to the shed vortices in the wake.

5.4 Results

5.4.1 Case 2.1

This section shows the results between the measurements and the engineering codes. Case 2.1

The following general observations can be made:

- The variation in axial force is not captured well by any of the codes.

- At 30% radius, there is a significant difference in normal force between the vortex line results and the BEM results where the vortex line method clearly is closer to the measurements.

- At 63% all codes are below the measurements. The variations in tangential force with azimuth are captured well by the vortex line code and the new BEM model.

- At 95% there is a good agreement in tangential force for the new BEM model and the vortex line code with the measurements.

The vortex line code does not capture the tower passage of the blade near 180 degrees azimuth

Figure 5-3. rotor axial force comparison for case 2.1

Figure 5-4. normal force and tangential force for case 2.1 at 30% radius

Figure 5-5 normal force and tangential force for case 2.1 at 63% radius

Figure 5-6 normal force and tangential force for case 2.1 at 95% radius

5.4.2 Case 2.2

The following general observations can be made:

- For the rotor axial force, the new BEM code and vortex line code agree well with the measurements where the old BEM code is significantly below the measurements

- At 30% radius, the normal force predicted by the vortex line code matches the measurements well. A larger discrepancy is found for the tangential force.

- At 63% radius, the trends in tangential force by the vortex line and new BEM code are in good agreement with the measurements but there is an offset in absolute value. The results for the normal force are inconclusive.

- At 95% radius, again the tangential force given by the new BEM code and vortex line code are captured well. An offset in normal force is found, but the trend with azimuth is predicted well by the new BEM and VortexLine code.
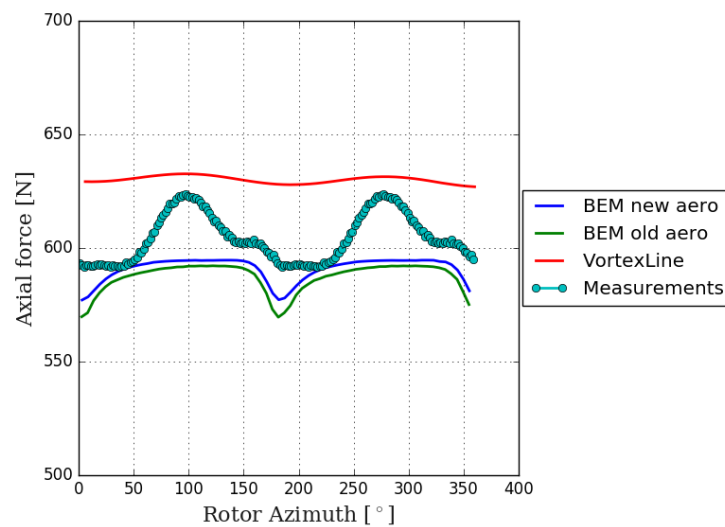
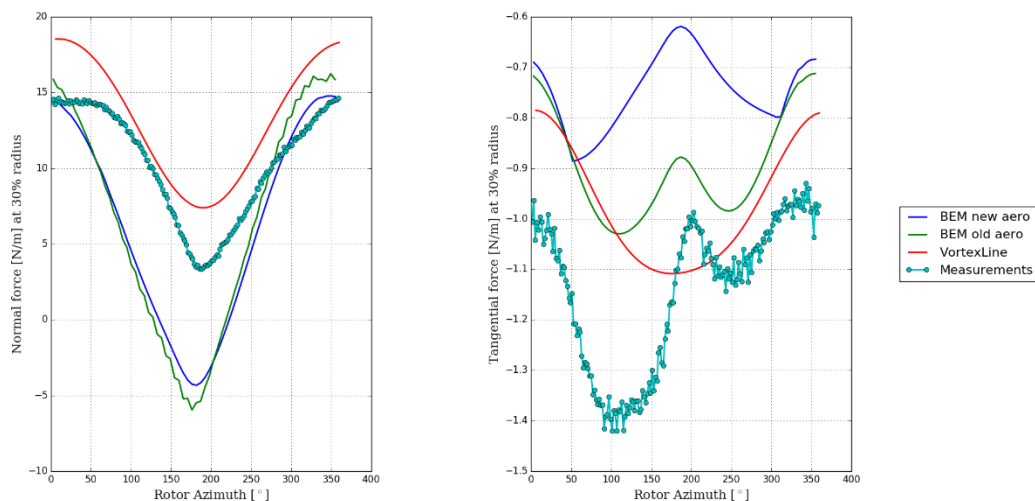**Figure 5-7. rotor axial force comparison for case 2.2**

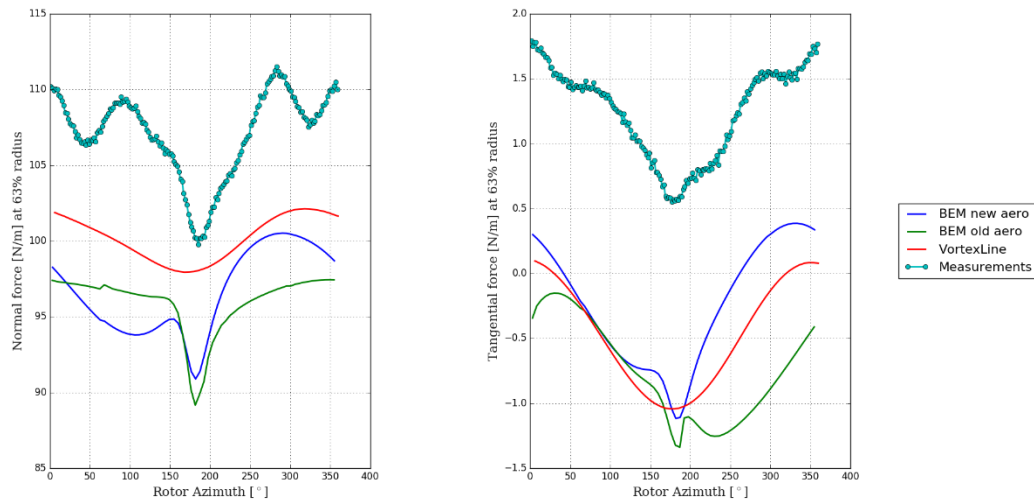**Figure 5-8. normal force and tangential force for case 2.2 at 30% radius**

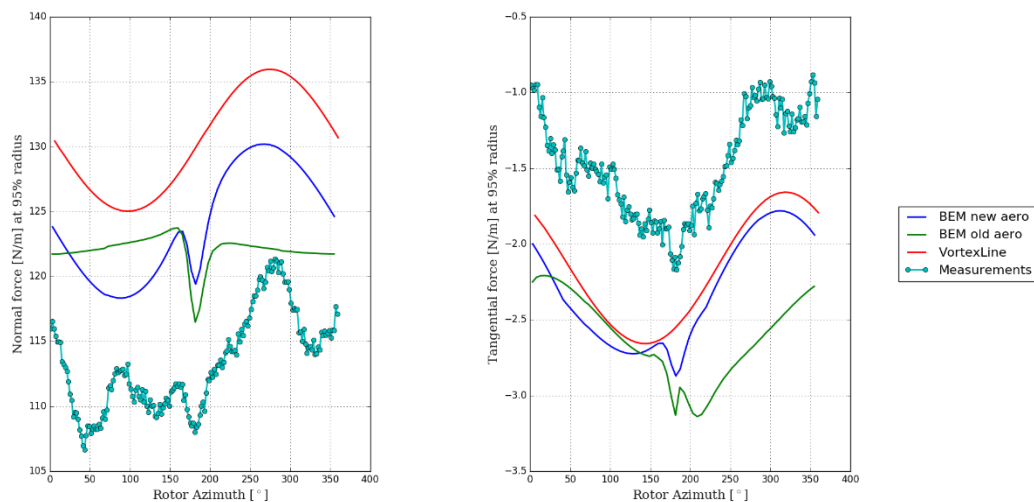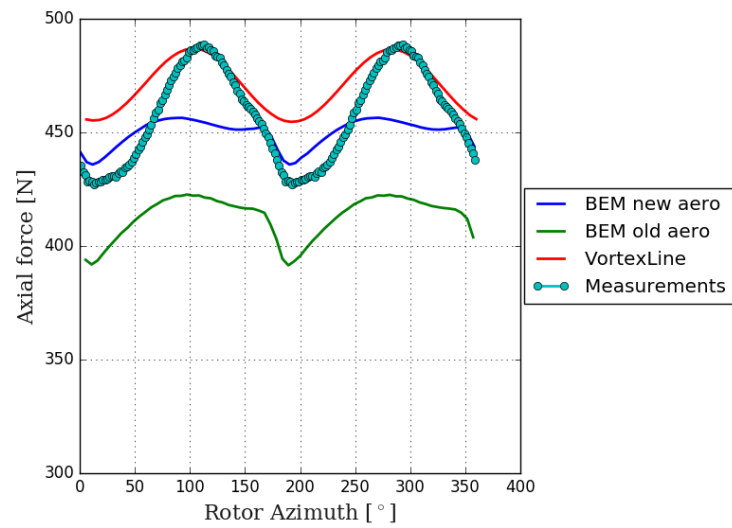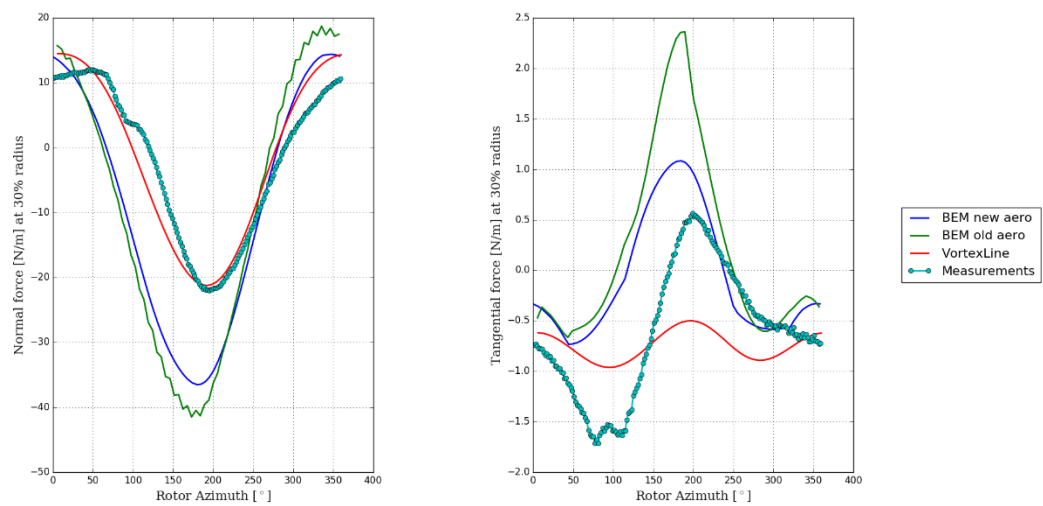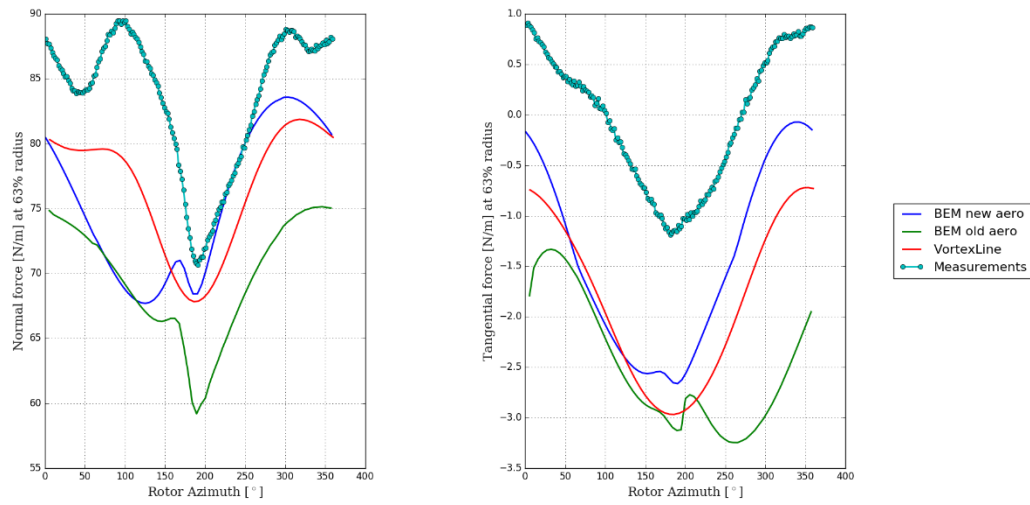**Figure 5-9 normal force and tangential force for case 2.2 at 63% radius**
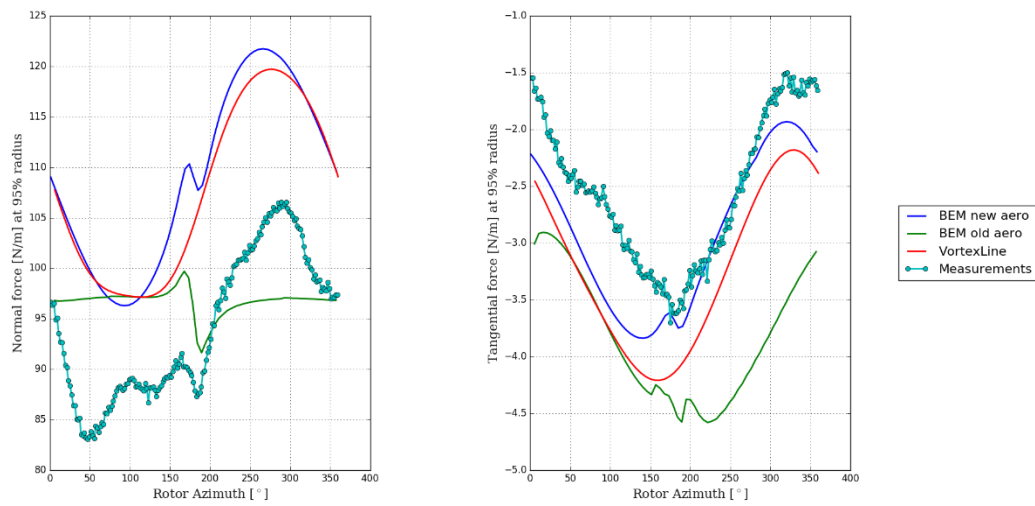
Figure 5-10 normal force and tangential force for case 2.2 at 95% radius

6 RERUNNING OF FULL LOAD SETS

This section describes a comparison campaign between the old and new aerodynamics codes using Bladed 4.7 and 4.8. The primary aim of this section is to identify results differences that are only caused by the differences in the aerodynamic models used. Discrepancies due to changes in other modelling features, such as the structural modelling, has been minimised by either using the same version of Bladed or by selecting appropriate model settings.

Two sets of comparisons are provided. First, a series of load sets from commercial projects have been rerun with Bladed 4.7 using the new and old aerodynamics code. This comparison is reported in Sections 6.2 and 6.3 and highlights the differences between the old and new aerodynamics implementations. Second, a comparison is made between the old aerodynamic results rerun using Bladed 4.7 and a re-run using Bladed 4.8. The setup of the Bladed 4.8 model was selected such that the new aerodynamics matched the old aerodynamics model as closely as possible. A discussion of the appropriate settings to achieve this is provided is provided in /16/ and the results of the comparison presented in Section 6.6.

6.1 Description of the cases

Commercial projects have been reanalysed using Bladed 4.7. The exact load results and turbine geometries cannot be disclosed in this report. Therefore, a summary of the relative differences in fatigue and extreme loading is presented. The following turbines have been used for testing:

- 3MW onshore turbine

- 2MW onshore turbine

- 2.5MW onshore turbine

- 6MW offshore turbine

- 5MW NREL wind turbine, using a jacket support structure

6.2 Fatigue loads

Table 6-1 summarizes the percentage differences found in Damage Equivalent Load (DEL) between the new and old aerodynamics. The most significant difference is found in the hub Fx fatigue for the 5MW NREL turbine. The likely cause is the fact that the new dynamic wake model provides a slower wake recovery which affects pitch-speed control loop stability and fore-aft aerodynamic damping. When the Pitt and Peters dynamic wake model was used, the difference in damage equivalent load is reduced to 9%. A controller retune to increase the pitch-speed loop stability would likely reduce the effect of the slower wake recovery.

Table 6-1 Percentage variation in DEL between new and old aero

Turbine	Blade root My (m=10)	Blade root Mx (m=10)	Rot Hub My(m=4)	Hub Fx (m=4)	Yaw bearing My (m=4)	Yaw bearing Mx (m=4)	Tower base My (m=4)
3MW onshore	-2.9%	0.2%	-0.4%	1.5%	-0.8%	-1.8%	-
2MW onshore	-1.4%	-14.7%	-1.8%	1.4%	-1.5%	-1.7%	1.3
2.5MW onshore	-1.1%	0.0%	-1.4%	-1.0%	-0.1%	-1.5%	-0.3%
6MW offshore	2.1%	0.5%	2.2%	0.9%	1.8%	1.2%	1.2%
5MW NREL	6.3%	0.6%	5.0%	15.3%	4.0%	1.0%	-

6.3 Extreme loads

Further, in the new aerodynamics more edgewise vibrations occurred in the dlc6.2 case where the rotor is idling at high wind speeds without the yaw system operational. For some wind directions, the blades are in deep stall where generally the aerodynamic damping is low or even negative. To remove the instabilities in the new aerodynamics the edgewise structural damping has been increased to 1.0-1.5%. Paragraph 6.4 discusses the source of these vibrations in more detail.

Table 6-2 summarises the percentage differences found in extreme load between the new and old aerodynamics. With some exceptions, the differences in extreme loads are generally within 10% but the differences are more significant than for the fatigue loads. In particular, the gust + direction change (dlc1.4) cases tend to become more driving. In Paragraph 6.5 a more in-depth analysis is presented on this load case.

Further, in the new aerodynamics more edgewise vibrations occurred in the dlc6.2 case where the rotor is idling at high wind speeds without the yaw system operational. For some wind directions, the blades are in deep stall where generally the aerodynamic damping is low or even negative. To remove the instabilities in the new aerodynamics the edgewise structural damping has been increased to 1.0-1.5%. Paragraph 6.4 discusses the source of these vibrations in more detail.

Table 6-2 Percentage variation in Ultimate load between new and old aerodynamics[1]

Turbine	Blade root Mxy	Blade root Mz	Hub Myz	Hub Fx	Yaw bearing Mxy	Yaw bearing Mz	Tower base Mxy	Tower Closest Approach (TCA)
3MW onshore	-2.65%	4.82%	-3.79%	-0.08%	4.16%	-0.97%	7.94%	23.8%
2MW onshore	-0.86%	2.31%	6.32%	-1.15%	5.05%	21.9%	1.97%	-2.2%
2.5MW onshore	-0.9%	0.3%	-3.4%	-0.5%	-7%	9.7%	2.6%	-2.4%
6MW offshore	2.4%	-1.6%	18.3%	0.3%	8.2%	21%	0.6%	-3%
5MW NREL	12.2%	6.2%	-0.14%	8.39%	0.87%	-5.3%	-	3.6%

6.4 Reduced aerodynamic damping in deep stall

As discussed in paragraph 6.3 the simulations using the new aerodynamics code experience more edgewise vibrations in idling conditions. In this paragraph the source of the vibrations is investigated in more detail.

6.4.1 Analysis of implementation differences

Both the new aerodynamics in Bladed 4.8 and the old aerodynamics in Bladed 4.7 contain an implementation of the Beddoes-Leishman dynamic stall model. Hence from that perspective there should not be significant differences in aerodynamic damping between the two models. This section highlights some key differences that may cause the changes in results.

Figure 6-1 shows the results of an aerodynamic experiment where a single aerofoil is oscillating in deep stall. The figure compares the resulting lift and drag hysteresis loops of the two different Beddoes-Leishman models. The old aerodynamics clearly shows, especially for the drag, a larger hysteresis loop. Figure 6-1 further shows that if the vortex lift term is removed the shape of the lift and drag loops changes significantly. In the 4.8 Incompressible Beddoes-Leishman the vortex lift term is only active

---

[1] Modal damping of edgewise modes increased to 1.0-1.5% for idling cases in storm conditions in combination with extreme yaw angles.

when the aerofoil ramps from attached flow into stall. Hence, in the current scenario, the 4.8 incompressible Beddoes-Leishman lift and drag loops have no vortex lift contribution.
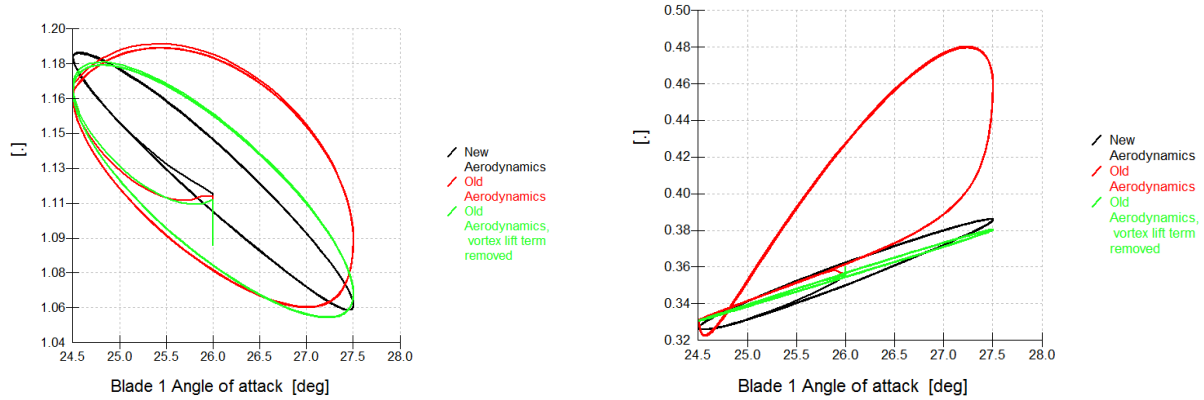
Figure 6-1 Comparison in lift (left) and drag (right) coefficient loops between old and new aerodynamics, $\alpha = 26° + 1.5°sin(1.257\pi t), V_\infty = 50m/s, c = 1m$

With the vortex lift term removed, the old aerodynamics still gives a larger hysteresis loop than the new code for the lift coefficient. The likely cause is the way the dynamic normal force coefficient is computed. In the old aerodynamics, the normal force coefficient is computed following the Kirchoff formulation:

$$C_n = C_n(\alpha) \left(\frac{1 + \sqrt{f}}{2} \right)^2 (\alpha - \alpha_0)$$

6.1

As found in reference /2, where f is the separation position. For the new aerodynamics, the following formulation is applied:

$$C_n = C_n(\alpha - \alpha_0)f + C_n^{fs}(\alpha)(1 - f)$$

6.2

Which is taken from /1, where C_n^{fs} is the normal force coefficient for fully separated flow.

Figure 6-2 illustrates how the unsteady lift when using either 6.2 or 6.1 to compute the normal force coefficient. The Original Kirchhoff formulation gives a wider hysteresis loop which will impact on the aerodynamic damping in deep stall conditions. (See Table 6-3) Note further that equation 6.1 is optionally included in Bladed 4.9 for the incompressible and compressible Beddoes-Leishman models

Based on the analyses in this paragraph the vortex lift term and expression for the normal force coefficient are earmarked as the primary sources for the change in aerodynamic damping in deep stall conditions when using either the 4.8 incompressible Beddoes-Leishman model or the 4.7 old aerodynamics model.
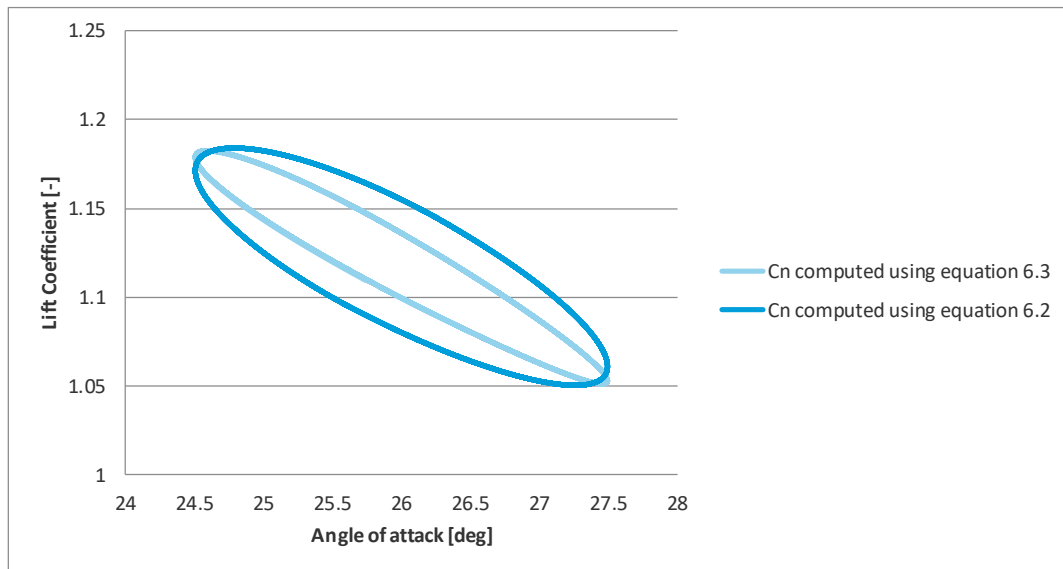
Figure 6-2 comparison in unsteady lift coefficient of new aerodynamics, $\alpha = 26° + 1.5°sin(1.257\pi t), V_\infty = 50m/s, c = 1m$

6.4.2 Time domain parked analysis

To illustrate the differences in damping between different model setups a parked simulation has been carried out with the rotor parked at a 30° yaw angle. The wind speed is ramped up from 0 to 50 m/s in the first 10s of the simulation. At 12s, a transient is applied on the wind direction with a period equal to the first blade edgewise frequency. Further the modal damping is set to zero.

The response in blade torsional tip rotation is plotted in **Error! Reference source not found.**. The incompressible Beddoes-Leishman model clearly gives a faster increase in tip rotation azimuth with time indicating that the oscillation is more negatively damped than the 4.7 aerodynamic model. In addition, in Bladed 4.8 an implementation is included that is equivalent to the Bladed 4.7 Beddoes-Leishman model. This equivalent implementation yields a nearly identical response as the original Bladed 4.7 simulation.
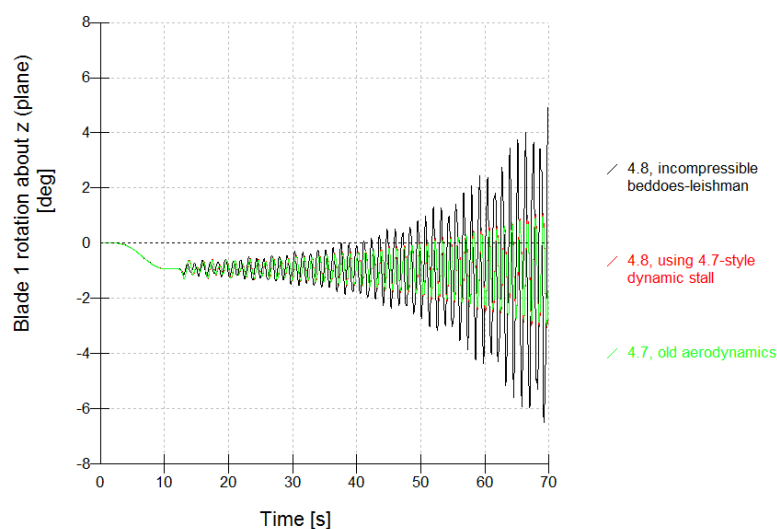
Figure 6-3 blade tip rotation, parked rotor, mean wind direction 30°, steady wind speed=50 m/s, structural damping = 0%

To interpret the results of **Error! Reference source not found.** in a more quantitative fashion, a system identification is carried out. It is assumed that the vibration in **Error! Reference source not found.** follows the relation:

$$x(t) = Ae^{-\xi\omega t}\sin(\omega t + \varphi) + x_0 \qquad\qquad 6.3$$

Using **Error! Reference source not found.** the parameters A, ξ,ω,φ and x0 are fitted to the time history using the evolutionary solver in Excel. The resulting damping ratio (ξ) and natural frequency are found in **Error! Reference source not found.**. The 4.8 incompressible Beddoes-Leishman gives around 46% lower damping than the baseline case. The frequency and damping of the 4.8 baseline case and the 4.7 old aerodynamics are nearly identical. Introducing the Kirchoff term improves the damping by 10-20%. Final using the multi-part blade model shows a significant increase in damping compared to all other settings.

Table 6-3 damping ratio and natural frequency of blade tip rotation of parked rotor, mean wind direction 30°, steady wind speed=50 m/s, structural damping = 0%

Configuration	Natural frequency [Hz]	Damping ratio [-]
4.8 baseline, pre-4.8 Beddoes-Leishman	0.833	-0.0076
4.7 old aerodynamics	0.833	-0.0077
4.8 incompressible Beddoes-Leishman	0.837	-0.0115
4.8 incompressible Beddoes-Leishman + Kirchoff	0.836	-0.0105
4.8 Multi-part, full geometric stiffness, pre-4.8 beddoes-leishman*	0.822	-0.0025

(*) used the blade x-deflection signal instead of tip rotation

Based on these results the following practise is recommended:

- Use Multi-Part blade by default for all simulations

- In 4.9 switch on the Kirchoff term when using (In)compressible Beddoes-Leishman

- If vibrations still occur in the parked/idling simulations, then the user can revert to the pre-4.8 Beddoes-Leishman model.

6.5 Simplified aerofoil orientation

From Bladed 4.8.0.52 an option is included named "Simplified aerofoil orientation". When selected, it is assumed that the aerofoil remains perpendicular to the blade root Z-axis when the blade is bending. This is equivalent to what is done in old aerodynamics. For highly bent blades this simplification can influence the blade inflow conditions and the subsequent loads.

It is found that this option can have a significant impact on the turbine loads for complex load cases like the gust+direction change case (dlc1.4). This is illustrated in Figure 6-4 and Figure 6-5 where the blade x-deflection and yaw bearing My is plotted for a gust + direction change around rated wind speed. Around 25s the Bladed 4.8 simulation shows a significantly larger peak in blade tip deflection. Switching on the simplified aerofoil orientation option brings the deflection more in line with Bladed 4.7. Further the differences are reduced if the skew wake correction method is switched off and "axial momentum" is used instead of "Glauert momentum". A similar trend is found in Figure 6-5 for the yaw bearing My load.
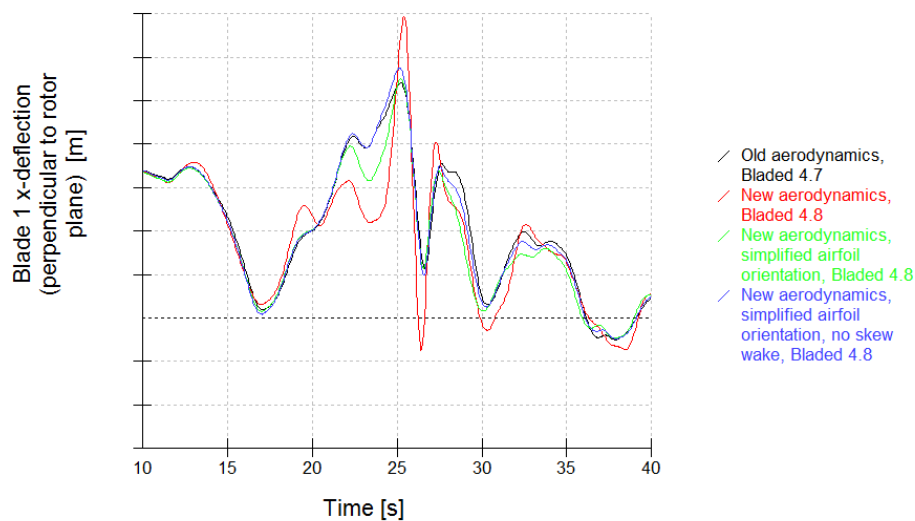
Figure 6-4 Blade x-deflection for dlc1.4 around rated wind speed, comparing old aerodynamics and new aerodynamics with and without simplified aerofoil orientation.
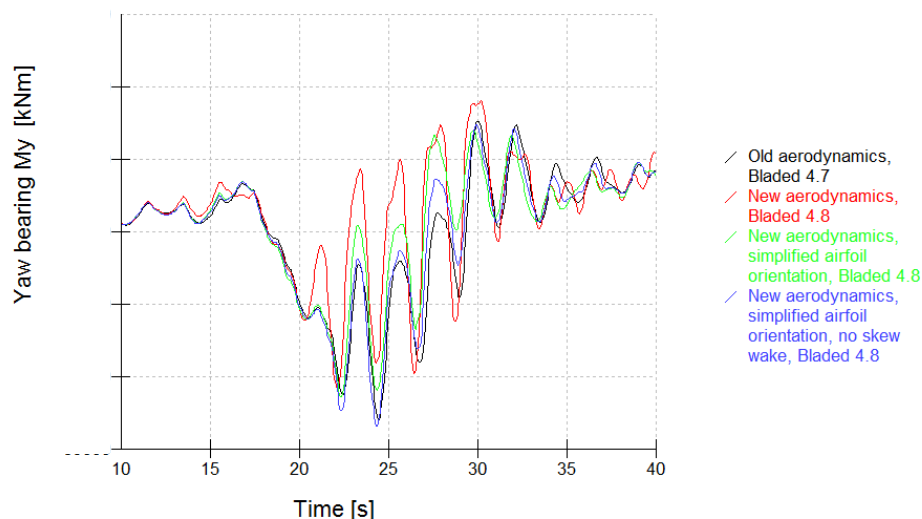
Figure 6-5 Yaw bearing My for dlc1.4 around rated wind speed, comparing old aerodynamics and new aerodynamics with and without simplified aerofoil orientation.

It is further found that the simplified aerofoil orientation method affects the aerodynamic damping in idling storm cases in large flow misalignment. It is found that damping is positively affected for positive angles of attack, but negatively for negative angles of attack. No validation on the "simplified aerofoil setting" is provided in this report. It is however considered more physically accurate to include the aerofoil rotation in the aerodynamic calculations and by default to disable the "simplified aerofoil orientation".

6.6 Rerunning load sets with aerodynamic settings to reproduce pre-4.8 results

In paragraph 6.2 and 6.3 the recommended default settings of the aerodynamic model are used. The user however can configure the aero dynamic settings such that these are equivalent to what is implemented in Bladed 4.7 and lower. An overview of these settings is presented in the Bladed user manual.

Table 6-4 presents the key fatigue load differences for the 3MW onshore turbibe. Generally differences in damage equivalent load are below 5%.

6.6.1   Fatigue loads

Table 6-4 Percentage variation in DEL between new and old aero

Turbine	Blade root My (m=10)	Blade root Mx (m=10)	Rot Hub My (m=4)	Hub Fx (m=4)	Yaw bearing My (m=4)	Yaw bearing Mx (m=4)	Tower base My (m=4)
3MW onshore	4.2%	0.5%	3.5%	4.6%	0.8%	2.6%	4.1%
2.5MW onshore	0.9%	0.1%	1.1%	1.5%	-0.1%	1.1%	3.3%

6.6.2

6.6.2   Extreme loads

Table 6-5 presents the extreme load results for the 3MW and 2.5MW onshore turbines. The maximum difference in extreme load is 6%. In these load simulations there has been no need to artificially increase the structural damping on the edgewise modes to prevent vibrations in idling simulations. In paragraph 6.4, and explanation is provided for the differences in edgewise damping predicted by the different implementations of the Beddoes-Leishman dynamic stall model.

Table 6-5 Percentage variation in Ultimate load between new and old aerodynamics

Turbine	Blade root Mxy	Blade root Mz	Hub Myz	Hub Fx	Yaw bearing Mxy	Yaw bearing Mz	Tower base Mxy	TCA
3MW onshore	0.8%	1.2%	-2.5%	-0.1%	-2.2%	0.5%	2.2%	-3.5%
2.5MW onshore	0.1%	-5.2%	-6.2%	0.8%	-1.4%	0.8%	3.5%	-5.6%

6.7   Effects of axial structural velocity induction on loads

When the turbine structure has a notable amount of movement in axial direction compared to the undisturbed wind speed, the standard induced velocity formulation in the momentum equation is no longer valid. This is important for floating wind turbines where large platform motions occur and in cases of turbine shutdown as a result of wind speed gusts, direction changes, fault cases, alarms etc. From Bladed 4.12 there is an option to include the axial structural velocity (StrucVel) for calculating the induced velocities. This term modifies the convective velocity used for the mass flux term in the momentum equations. To demonstrate the influence of this physical aspect, two test cases are defined and tested in this report:

Case-A

A1. Reference: the simulation was carried out for a stationary turbine exposed to a constant wind speed of 7 m/s rotating at a constant rotational speed of 10 rpm. Simulated using Bladed 4.12 with/without StrucVel.

A2. Old model: the simulation was carried out for a turbine exposed to a constant wind speed of 6 m/s rotating at a constant rotational speed of 10 rpm. The turbine structure is artificially accelerated in negative axial direction by 1 m/s^2 for 1s before the acceleration is set to zero. This leads to a constant relative wind speed of 7 m/s (6 m/s from the wind + 1 m/s from the structure). This case was simulated using Bladed 4.12 without StrucVel.

A3. New model: the setup is exactly the same as Test A2 but StrucVel is active.

Case-B

B1. Reference: the simulation was carried out for a stationary turbine exposed to an oscillating wind speed with an amplitude of 0.3 m/s around a mean wind speed of 5 m/s and at a frequency of 0.1 Hz. The turbine rotor rotates at a constant rotational speed of 10 rpm. This test case was simulated using Bladed 4.12 with/without StrucVel.

B2. Old model: the simulation was carried out for a turbine exposed to a constant wind speed of 5 m/s rotating at a constant rotational speed of 10 rpm. A sinusoidal structural acceleration in axial direction was applied on the whole turbine structure such that the turbine sees exactly the same relative velocity as that in Test B1. This case was simulated using Bladed 4.12 without StrucVel.

B3. New model: the setup is exactly the same as Test B2 but StrucVel is active.

Figure 6-6 Comparison between different Bladed runs for Case-A; relative axial wind speed (left) and sectional axial force at r = 26.407 m (right); Reference (Case A1), Old Model (Case A2), New Model (Case A3).
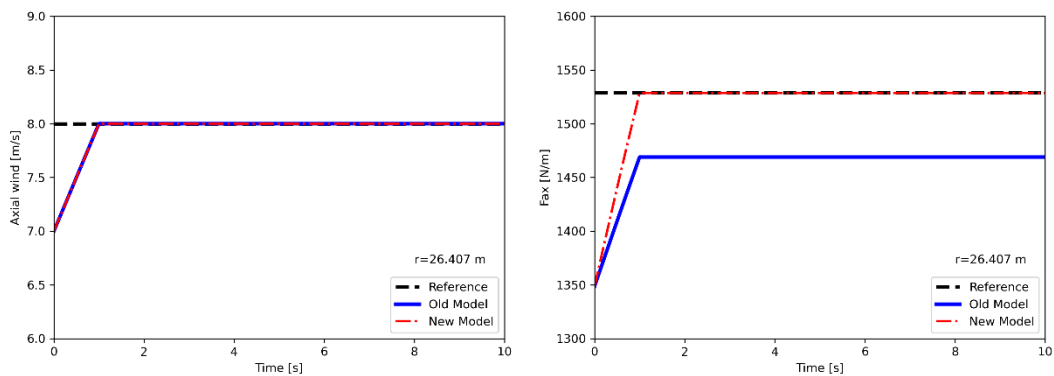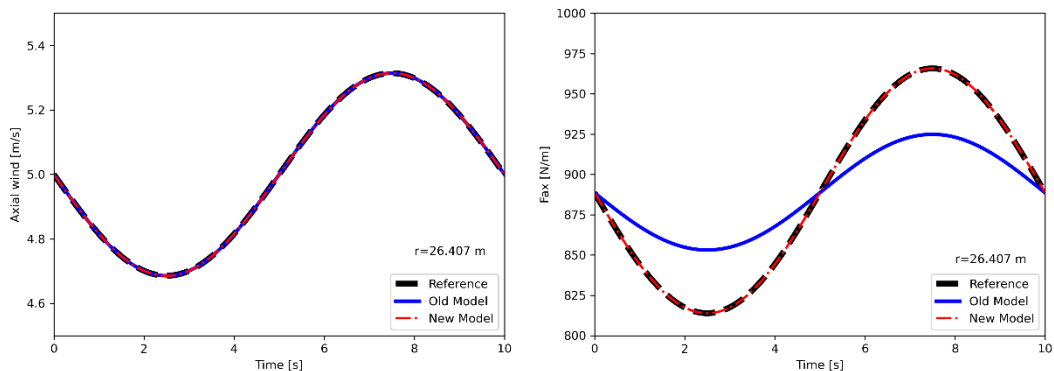

Figure 6-7 Comparison between different Bladed runs for Case-B; relative axial wind speed (left) and sectional axial force at r = 26.407 m (right); Reference (Case B1), Old Model (Case B2), New Model (Case B3).

The comparison results for Case-A are presented Figure 6-6. One can see that all tests match the relative undisturbed axial wind speed for time greater than 1 s. Physically all tests shall generate the same axial force component. Despite that, if the axial structural velocity component is not included in the induction calculation, the resulting axial force in Case A2 is much lower than the expected reference value (Case A1). By enabling StrucVel in Case A3, the simulation results are greatly improved and match the reference data. A similar characteristic is observed for Case-B in Figure 6-7 that physically models the surging motion of floating wind turbines. It can be observed that the amplitude of the axial force component in Case B2 is not correctly predicted by the old model although the relative undisturbed axial velocities are the same as the reference in Case B1. This effect is taken into account using the improved model by activating the axial structural velocity induction option in Bladed. For the improved model in Case B3, a good agreement with the reference data is observed.

Table 6-6 Percentage variation in DEL between Bladed 4.12 without and with inclusion of the axial structural velocity

Turbine	Blade root My (m=10)	Blade root Mx (m=10)	Rot Hub My (m=4)	Hub Fx (m=4)	Yaw bearing My (m=4)	Yaw bearing Mx (m=4)	Tower base My (m=4)
8MW offshore (Windows)	-0.53%	0.00%	-0.48%	-0.05%	-0.20%	-0.18%	-0.10%
8MW offshore (Linux)	-0.53%	0.00%	-0.48%	-0.04%	-0.23%	-0.17%	-0.12%
2.5MW onshore (Windows)	0.10%	-0.03%	0.58%	0.20%	0.21%	0.35%	0.70%
2.5MW onshore (Linux)	0.13%	-0.04%	0.60%	0.17%	0.21%	0.49%	0.66%

Table 6-7 Percentage variation in extreme load between Bladed 4.12 without and with inclusion of the axial structural velocity

Turbine	Blade root Mxy	Blade root Mz	Hub Myz	Hub Fx	Yaw bearing Mxy	Yaw bearing Mz	Tower base Mxy
8MW offshore (Windows)	0.06%	-0.16%	0.47%	-0.11%	0.32%	0.28%	-0.07%
8MW offshore (Linux)	0.06%	-0.16%	0.49%	-0.07%	0.34%	0.31%	-0.07%
2.5MW onshore (Windows)	0.48%	0.43%	0.01%	0.39%	-0.21%	0.54%	0.23%
2.5MW onshore (Linux)	0.50%	0.14%	0.16%	0.37%	-0.22%	0.48%	0.24%

To further quantify the influence of the axial structural velocity induction on resulting loads, a load analysis has been carried out using two real turbine models. This provides an estimate of how much ultimate and fatigue loads will change due to this refinement in the aerodynamics calculations. Table 6-6 and Table 6-7 present the summarized loadset calculation data in terms of the fatigue and extreme load cases, respectively. Although in most load parameters the results are not likely affected (< 0.5%), the load analysis shows that the inclusion of the axial structural velocity slightly influences the blade root

flapwise moments, rotating hub My and tower base My. These most affected cases are shut downs due to environmental conditions. The benefit of having the correction term included will be more likely of greater significance when the structural motion is stronger such as for floating wind turbines. A loadset analysis for floating wind turbines has not been completed and therefore an indication of the change in load level cannot be provided in the present report.

6.8 Dynamic power curve

In section 3 it is shown that the steady aerodynamic power is nearly identical for the new and old aerodynamics codes. However, in the dynamic case, the specifics of dynamic wake and dynamic stall modelling plays a significant role. Furthermore, the flow misalignment due to a turbulent wind field will have an impact on the power production due to the presence or absence of a skew wake correction model.

In this section, a comparison in dynamic power is presented using six turbulent wind speeds per wind bin and using a GL2010 normal turbulence model.

Figure 6-8 shows the percentage difference in electrical power as a function of mean wind speed for the 3MW onshore turbine. The differences in power are most significant for the lower wind speeds. It is likely this is caused by higher turbulence levels causing larger yaw misalignment and therefore differences in power production. The former is confirmed when the comparison is rerun using axial momentum theory and switching off the skew wake model. These actions bring the mean power levels more in line with the old aerodynamics.
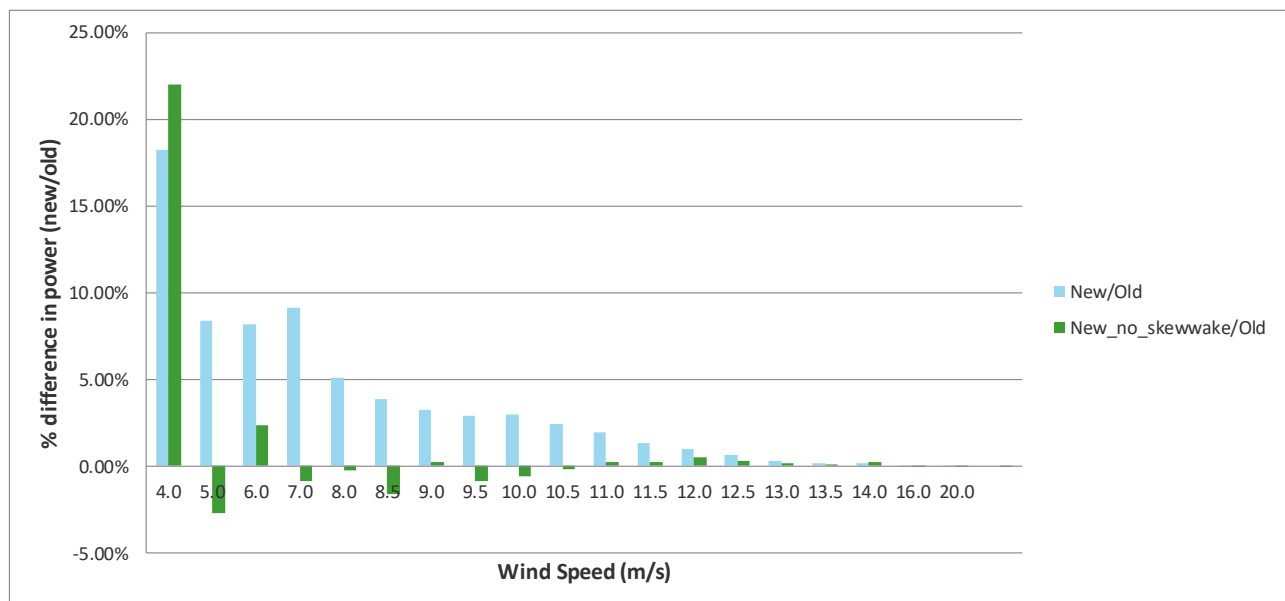

Figure 6-8 Percentage difference in mean dynamic power as a function of wind speed, 3MW onshore turbine, six turbulent seeds per wind bin used.

7 VALIDATION OF NEW AERODYNAMICS WITH NON-LINEAR BLADE MODELLING

This section presents the results of a validation campaign of Bladed 4.7 with new aerodynamics and a non-linear blade model (also called "multi-part" blade) against measurements on the GE Haliade 6MW turbine.

The following figures show the comparison between simulated and measured loads as a function of wind speed. The simulations in Bladed have been run with 11% turbulence using a Kaimal turbulence model.

The plots shown in this section were originally presented in /15/.

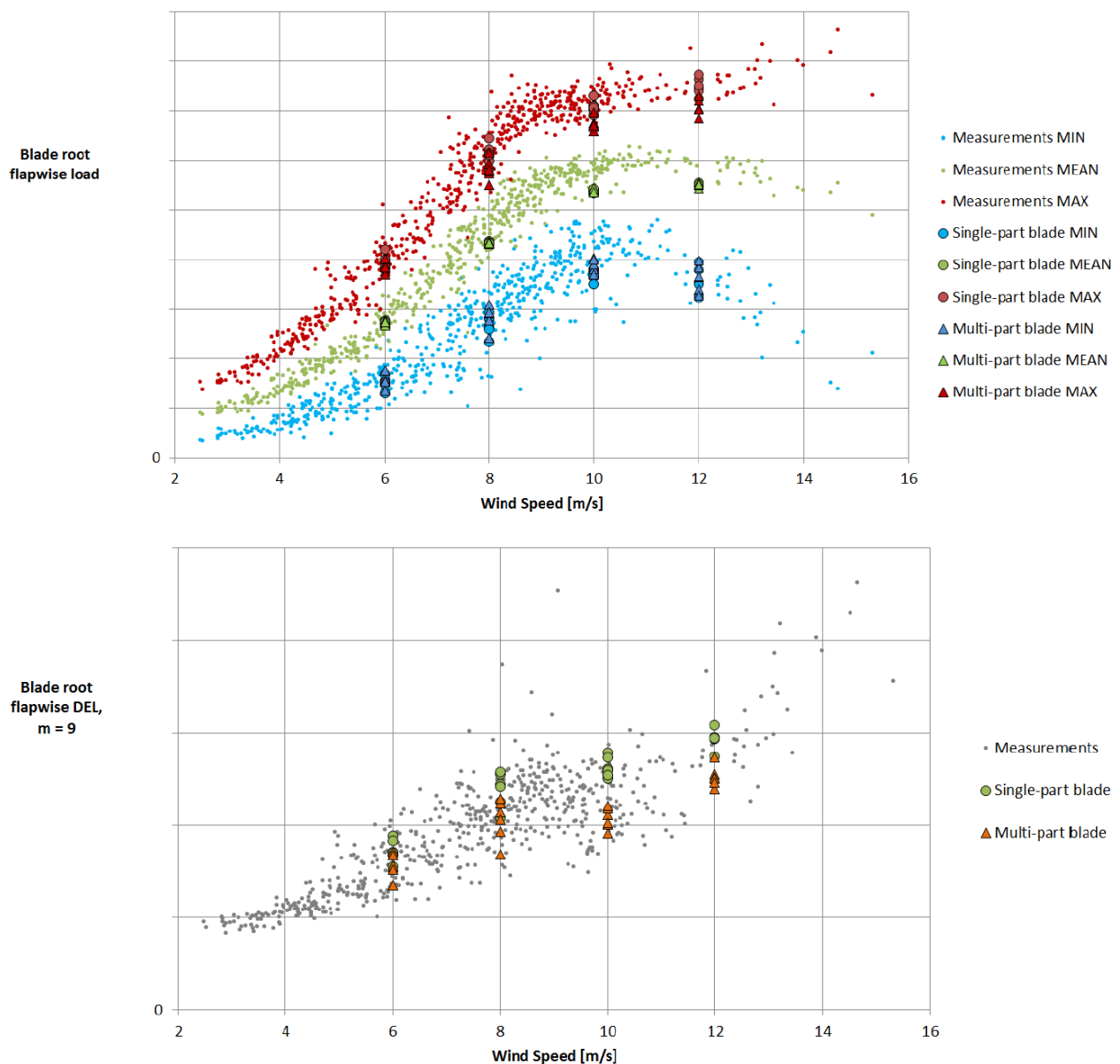## 7.1 Comparison of simulated loads against measurements

Figure 7-1 Comparison in flapwise blade bending moment, GE measurements and Bladed
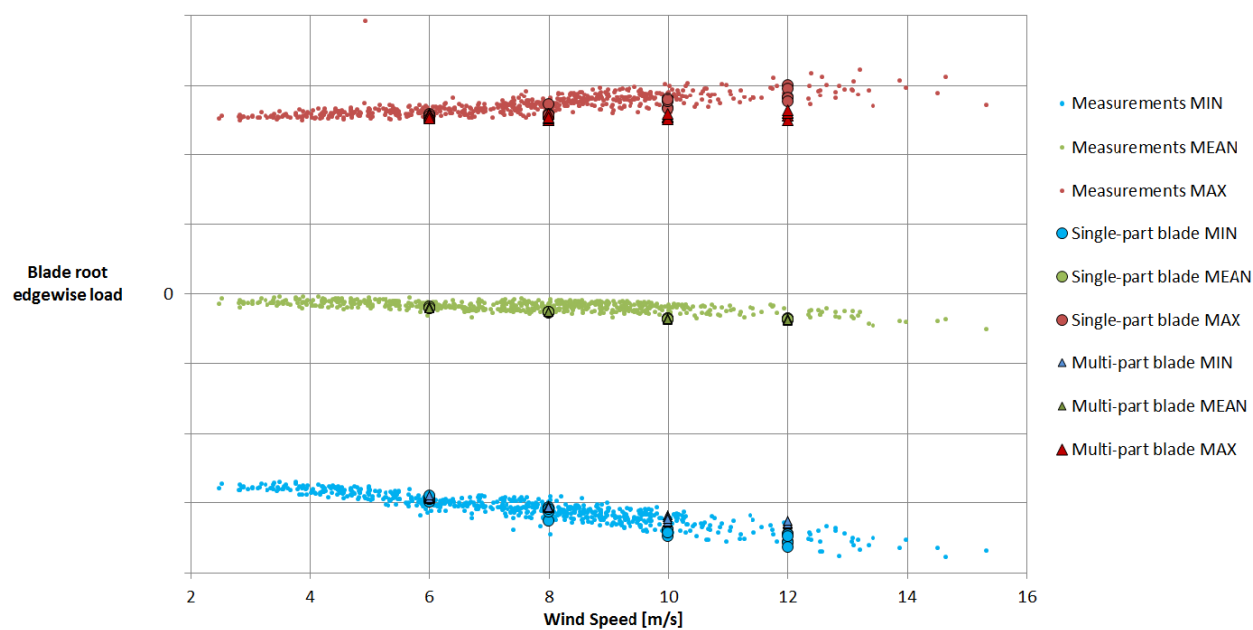
Figure 7-2 Comparison in edgewise blade bending moment, GE measurements and Bladed
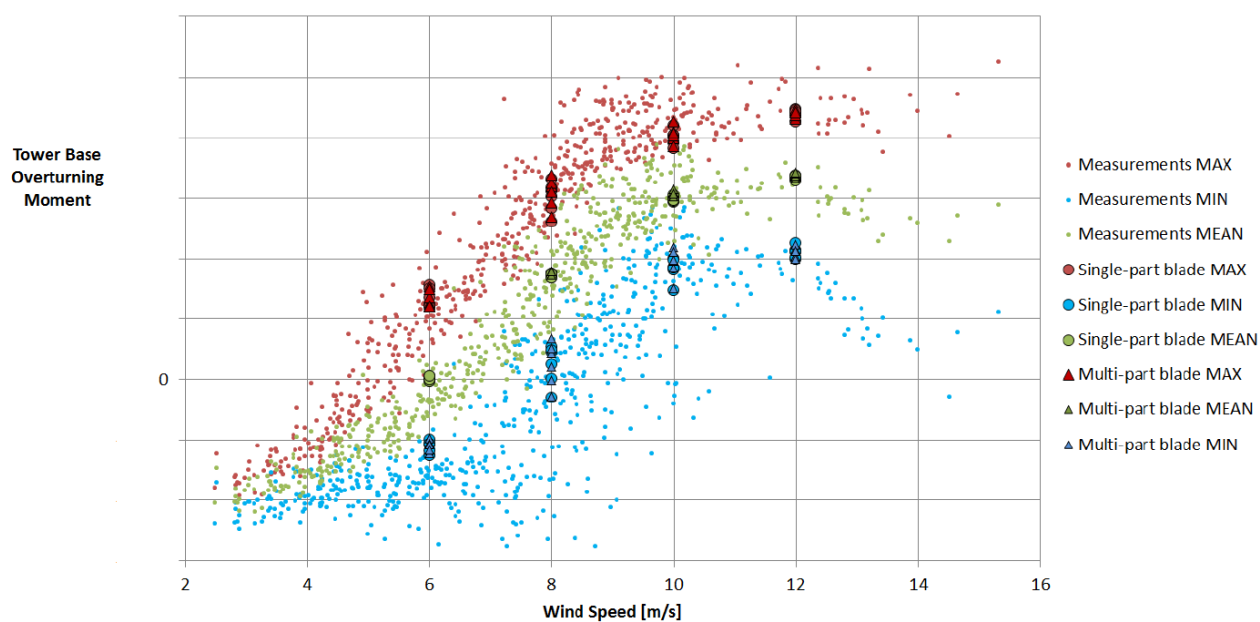

Figure 7-3 Comparison in tower base bending moment, GE measurements and Bladed

8 REFERENCES

/1/ Hansen, M.H., Gaunaa, M., and Madsen, H.Aa., "*A Beddoes-Leishman type dynamic stall model in state-space and indicial formulations*". Technical report Risø-R-1354(EN), Risø National Laboratory, Roskilde, June 2004

/2/ Leishman J.G. and Beddoes T. S. , "A semi-empirical model for dynamic stall", *Journal of the American Helicopter Society*, July 1989

/3/ Unsteady Aerodynamics Experiment Phase VI: Wind Tunnel Test Configurations and Available Data Campaigns, NREL/TP-500-29955, December 2001

/4/ M.H.M. Kloosterman, Development of the free wake behind a horizontal axis wind turbine, Msc Thesis, *Delft University of Technology*, July 2009

/5/ W. Collier, Comparison of Bladed versions 4.5 and 4.6, *GH internal report*, June 2014

/6/ www.mexnext.org , visited at 24-02-2015

/7/ J. B. de Vaal, M. O. L. Hansen, and T. Moan, Effect of wind turbine surge motion on rotor thrust and induced velocity *Wind Energy Vol 17*, 2014

/8/ Øye, S., "TUDK model". In *Joint Investigation of Dynamic Inflow Effects and Implementation of an Engineering Method*, Appendix N, edited by H. Snel and J.G. Schepers, Petten, 1995

/9/ Witold Skrzypiński, Analysis and modeling of unsteady aerodynamics with application to wind turbine blade vibration at standstill conditions, Ph.D. Thesis, DTU Wind Energy, February 2012

/10/ J.G. Leishman, State-Space model of unsteady airfoil behaviour and dynamic stall, In Center for Rotorcraft Education and Research, 1989

/11/ DNV GL, Theory Manual Bladed, Version 4.7, June 2015

/12/ DNV GL, Multi-Part Blade Beta: User Guide for Bladed 4.7, March 2016

/13/ User Guide and Verification of Linearisation module in Bladed 4.8, March 2018

/14/ ECN-E--14-060, Final report of IEA Wind Task 29: Mexnext (Phase 2), December 2014

/15/ W Collier, J Milian Sanz. "Comparison of linear and non-linear blade model predictions in Bladed to measurement data from GE 6MW wind turbine". Torque from Wind 2016

/16/ DNV GL, User Manual Bladed, Version 4.7, June 2015

ABOUT DNV GL

Driven by our purpose of safeguarding life, property and the environment, DNV GL enables organizations to advance the safety and sustainability of their business. We provide classification and technical assurance along with software and independent expert advisory services to the maritime, oil and gas, and energy industries. We also provide certification services to customers across a wide range of industries. Operating in more than 100 countries, our 16,000 professionals are dedicated to helping our customers make the world safer, smarter and greener.